Remote sensing phenology at European northern latitudes - From ground spectral towers to satellites

Jin, Hongxiao

2015

Remote sensing phenology at European northern latitudes

From ground spectral towers to satellites

Hongxiao Jin
Department of Physical Geography and Ecosystem Science | LUND UNIVERSITY

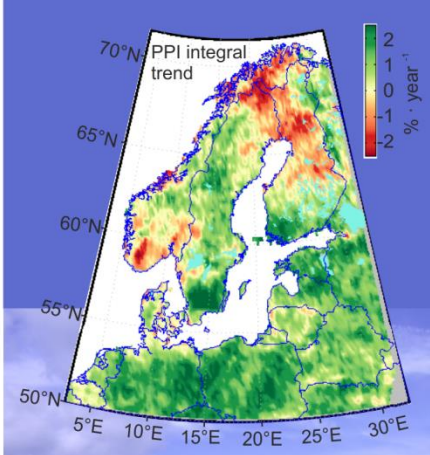

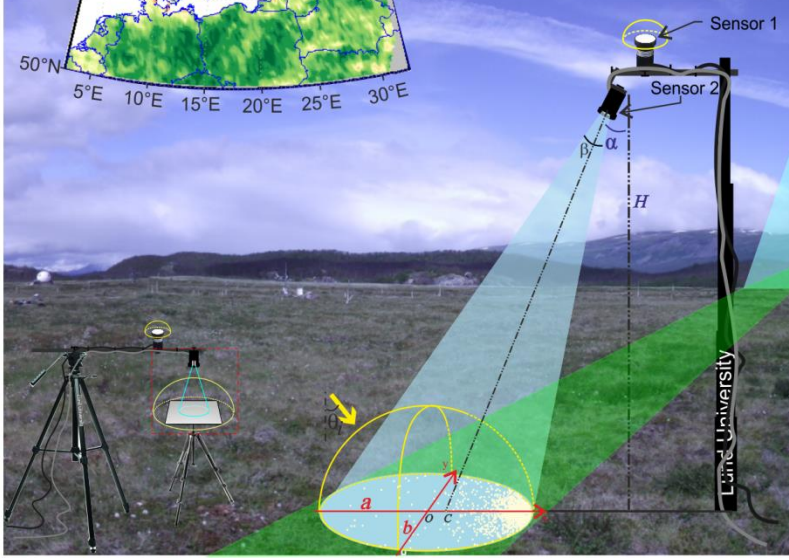

Remote sensing phenology at European northern latitudes

From ground spectral towers to satellites

Hongxiao Jin

DOCTORAL DISSERTATION
by due permission of the Faculty of Science, Lund University, Sweden.

To be defended at Världen auditorium. Thursday the 11th of June, 2015 at 10:00.

Faculty opponent

Professor Pauline Stenberg
Department of Forest Sciences, University of Helsinki

Organization

LUND UNIVERSITY

Department of Physical Geography and Ecosystem Science, Sölvegatan 12, SE-223 62, Lund, Sweden

Author(s) Hongxiao Jin

Document name

DOCTORAL DISSERTATION

Date of issue 2015-05-15

Sponsoring organization
Swedish Research Council Formas

Title and subtitle: Remote sensing phenology at European northern latitudes — From ground spectral towers to satellites

Abstract

Plant phenology exerts major influences on carbon, water, and energy exchanges between atmosphere and ecosystems, provides feedbacks to climate, and affects ecosystem functioning and services. Great efforts have been spent in studying plant phenology over the past decades, but there are still large uncertainties and disputations in phenology estimation, trends, and its climate sensitivities. This thesis aims to reduce these uncertainties through analyzing ground spectral sampling, developing methods for *in situ* light sensor calibration, and exploring a new spectral index for reliable retrieval of remote sensing phenology and climate sensitivity estimation at European northern latitudes.

The ground spectral towers use light sensors of either nadir or off-nadir viewing to measure reflected radiation, yet how plants in the sensor view contribute differently to the measured signals, and necessary *in situ* calibrations are often overlooked, leading to great uncertainties in ground spectral sampling of vegetation. It was found that the ground sampling points in the sensor view follow a Cauchy distribution, which is further modulated by the sensor directional response function. We proposed *in situ* light sensor calibration methods and showed that the user *in situ* calibration is more reliable than manufacturer's lab calibration when our proposed calibration procedures are followed. By taking the full advantages of more reliable and standardized reflectance, we proposed a plant phenology vegetation index (PPI), which is derived from a radiative transfer equation and uses red and near infrared reflectance in calculation. PPI showed good linearity with canopy green leaf area index, and is correlated with gross primary productivity, better than other vegetation indices in our test. With suppressed snow influences, PPI shows great potentials for retrieving phenology over coniferous-dominated boreal forests. PPI was used to retrieve plant phenology from MODIS nadir BRDF-adjusted reflectance at European northern latitudes for the period 2000-2014. We estimated the trend of start of growing season (SOS), end of growing season (EOS), length of growing season (LOS), and the PPI integral for the time span, and found significant changes in most part of the region, with an average rate of -0.39 days·year^{-1} in SOS, 0.48 days·year^{-1} in EOS, 0.87 days·year^{-1} in LOS, and 0.79%·year^{-1} in the PPI integral over the past 15 years. We found that the plant phenology was significantly affected by climate in most part of the region, with an average sensitivity to temperature: SOS at -3.43 days·°C^{-1}, EOS at 1.27 days·°C^{-1}, LOS at 3.16 days·°C^{-1}, and PPI integral at 2.29 %·°C^{-1}, and to precipitation: SOS at 0.28 days·cm^{-1}, EOS at 0.05 days·cm^{-1}, LOS at 0.04 days·cm^{-1}, and PPI integral at -0.07%·cm^{-1}. These phenology variations were significantly related to decadal variations of atmospheric circulations, including the North Atlantic Oscillation and the Arctic Oscillation.

The methods developed in this thesis can help to improve the reliability of long-term field spectral measurements and to reduce uncertainties in remote sensing phenology retrieval and climate sensitivity estimation.

Key words Remote sensing, northern latitude, Plant phenology index (PPI), ground spectral tower, calibration, climate sensitivity.

Classification system and/or index terms (if any)

Supplementary bibliographical information

Language: English

ISSN and key title

ISBN
978-91-85793-49-5

Recipient's notes

Number of pages 174

Price

Security classification

Remote sensing phenology at European northern latitudes

From ground spectral towers to satellites

Hongxiao Jin

LUND
UNIVERSITY

A doctoral thesis at a university in Sweden is produced either as a monograph or as a collection of papers. In the latter case the introductory part constitutes the formal thesis, which summarizes the accompanying papers already published or manuscripts at various stages (in press, submitted, or in preparation).

Cover design by Hongxiao Jin. Terra-MODIS sensor and ground spectral tower over the landscape of Stordalen mire in Abisko of northern Sweden. Together with sketch figure of *in situ* calibration of multispectral sensors, and final results of PPI trend map 2000-2014.

Department of Physical Geography and Ecosystem Science
Faculty of Science, Lund University

ISBN 978-91-85793-49-5

Printed in Sweden by Media-Tryck, Lund University
Lund 2015

List of papers

I. Eklundh, L., Jin, H., Schubert, P., Guzinski, R., & Heliasz, M. (2011). An optical sensor network for vegetation phenology monitoring and satellite data calibration. *Sensors*, 11, 7678-7709

II. Jin, H., & Eklundh, L. (2015). *In Situ* Calibration of Light Sensors for Long-Term Monitoring of Vegetation. *Geoscience and Remote Sensing, IEEE Transactions on*, 53, 3405-3416

III. Jin, H., & Eklundh, L. (2014). A physically based vegetation index for improved monitoring of plant phenology. *Remote Sensing of Environment*, 152, 512-525

IV. Jin, H., A. M. Jönsson, C. Olsson, J. Linström, P. Jönsson, K. Bolmgren, O. Langvall, L. Eklundh, Plant phenology trends at European northern latitudes and relationships with climate variability. *Manuscript*.

List of contributions

I. HJ developed the measurement theory, contributed to the field work, data analysis and interpretation together with the co-authors; wrote the first draft of the paper (except Introduction), with subsequent improvements by the co- authors.

II. HJ led the design of the study, carried out all calibration experiments, field work numerical simulations, uncertainty analysis and wrote the first draft of the paper, with significant revision and improvement by the co-author.

III. HJ led the design of the study, carried out all theoretical research, numerical modelling, field experiment on leaf-stack, and interpretation of the results; proposed the PPI with the co-author and wrote the first draft of the paper, with significant improvement by the co-author.

IV. HJ led the design of the study, revised TIMESAT software by parallel programming with OpenMP, Matlab MEX programming mixed with Fortran, and adding one more threshold method, and processed the data. HJ performed all data analyses, and wrote the first draft of the paper, with improvement by the co-authors.

Abstract

Plant phenology exerts major influences on carbon, water, and energy exchanges between atmosphere and ecosystems, provides feedbacks to climate, and affects ecosystem functioning and services. Great efforts have been spent in studying plant phenology over the past decades, but there are still large uncertainties and disputations in phenology estimation, trends, and its climate sensitivities. This thesis aims to reduce these uncertainties through analyzing ground spectral sampling, developing methods for *in situ* light sensor calibration, and exploring a new spectral index for reliable retrieval of remote sensing phenology and climate sensitivity estimation at European northern latitudes.

The ground spectral towers use light sensors of either nadir or off-nadir viewing to measure reflected radiation, yet how plants in the sensor view contribute differently to the measured signals, and necessary *in situ* calibrations are often overlooked, leading to great uncertainties in ground spectral sampling of vegetation. It was found that the ground sampling points in the sensor view follow a Cauchy distribution, which is further modulated by the sensor directional response function. We proposed *in situ* light sensor calibration methods and showed that the user *in situ* calibration is more reliable than manufacturer's lab calibration when our proposed calibration procedures are followed.

By taking the full advantages of more reliable and standardized reflectance, we proposed a plant phenology vegetation index (PPI), which is derived from a radiative transfer equation and uses red and near infrared reflectance. PPI shows good linearity with canopy green leaf area index, and is correlated with gross primary productivity, better than other vegetation indices in our test. With suppressed snow influences, PPI shows great potentials for retrieving phenology over coniferous-dominated boreal forests.

PPI was used to retrieve plant phenology from MODIS nadir BRDF-adjusted reflectance at European northern latitudes for the period 2000-2014. We estimated the trend of start of growing season (SOS), end of growing season (EOS), length of growing season (LOS), and the PPI integral for the time span, and found significant changes in most part of the region, with an average rate of -0.39 days·year^{-1} in SOS, 0.48 days·year^{-1} in EOS, 0.87 days·year^{-1} in LOS, and 0.79%·year^{-1} in the PPI integral over the past 15 years. We found that the plant phenology was significantly affected by climate in most part of the region, with an average sensitivity to temperature: SOS at -3.43 days·°C^{-1}, EOS at 1.27 days·°C^{-1},

LOS at 3.16 days·°C^{-1}, and PPI integral at 2.29 %·°C^{-1}, and to precipitation: SOS at 0.28 days·cm^{-1}, EOS at 0.05 days·cm^{-1}, LOS at 0.04 days·cm^{-1}, and PPI integral at -0.07%·cm^{-1}. These phenology variations were significantly related to decadal variations of atmospheric circulations, including the North Atlantic Oscillation and the Arctic Oscillation.

The methods developed in this thesis can help to improve the reliability of long-term field spectral measurements and to reduce uncertainties in remote sensing phenology retrieval and climate sensitivity estimation.

Sammanfattning

Växters fenologi påverkar ekosystemens funktion och tjänster, och återkopplar till klimatet genom att påverka utbytet av kol, vatten och energi mellan atmosfär och ekosystem. Under de senaste decennierna har växternas fenologi studerats i allt större omfattning, men fortfarande är osäkerheten stor och enighet saknas om klimatets inverkan på fenologi och förändringar över tiden. Detta projekt syftar till att minska osäkerheterna genom att analysera marknära insamling av spektrala data, utveckla nya metoder för kalibrering av ljussensorer i fält, och utforska nya spektralindex för mer tillförlitlig uppskattning av växternas fenologi och klimatkänslighet i norra Europa med hjälp av fjärranalysdata.

Vid fältstationer används ofta sensorer med lodrät eller sned vinkel för att mäta reflekterad strålning, men ofta är osäkerheten i mätningarna stor då nödvändig fältkalibrering av sensorerna saknas, och därigenom förbises hur olika växter påverkar den uppmätta reflektionen. Våra resultat tyder på att växternas reflektion följer en Cauchy-fördelning, modifierad av sensorns geometriska responsfunktion. Vi utvecklade en metod för fältkalibrering av spektralsensorer och visade hur denna metod ökar trovärdigheten av mätningarna gentemot mätningar gjorda med tillverkarnas standardkalibreringar.

Med mer trovärdiga reflektionsmätningar utvecklade vi ett fenologiskt vegetationsindex (PPI) som beräknas genom en strålningsekvation baserat på röd och nära-infraröd reflektion. PPI var linjärt korrelerad med trädensbladyteindex (LAI, leaf area index) och var bättre korrelerad med brutto- primärproduktion än andra vegetationsindex. PPI har speciellt stor potential för barrträdsdominerad boreal skog eftersom PPI är mindre känslig för påverkan av snö än andra vegetationsindex.

Vi uppskattade fenologin över norra Europa mellan 2000 och 2014 med PPI beräknat med s.k. BRDF-justerad reflektion från MODIS-sensorn. Vi utvärderade förändringar i växtsäsongens start (SOS), slut (EOS), längd (LOS) och PPI-integral och kunde påvisa signifikanta förändringar under de senaste 15 åren i större delen av norra Europa. I snitt var förändringen -0.39 dagar·år^{-1} för SOS, 0.48 dagar·år^{-1} för EOS, 0.87 dagar·år^{-1} för LOS, och 0.79%·år^{-1} för PPI-integralen. Fenologin var i de flesta områden signifikant påverkad av klimatet, i relation till temperatur; -3.43 dagar·°C^{-1} för SOS, 1.27 dagar·°C^{-1} för EOS, 3.16 dagar·°C^{-1} för LOS, och 2.29 %·°C^{-1} för PPI-integralen, och till nederbörd; 0.28 dagar·cm^{-1} för SOS, 0.05 dagar·cm^{-1} för EOS, 0.04 dagar·cm^{-1} för LOS

och -0.07%·cm^{-1} för PPI-integralen. Dessa förändringar var signifikant relaterade till variationer över de senaste årtiondena av atmosfäriska cirkulationsmönster, såsom den Nordatlantiska oscillationen och den Arktiska oscillationen.

Metoderna som har utvecklats i detta projekt ökar trovärdigheten av spektralmätningar och minskar osäkerheten i estimerad fenologi och klimatkänslighet baserad på fjärranalysdata.

中文摘要

植物物候对生态系统和大气之间的碳、水循环以及能量交换有着重要影响。植物的季节性变化，例如树冠叶面指数，以及相应产生的地面能量反射系数、树冠蒸腾效率和其它生物物理参数的增减，对气候系统有重要的反馈作用，从而影响其它生物的季节性生长、协调和竞争活动和现实生态位细分，并对生态系统的功能和服务产生重要作用。为了重建全球及区域性近几十年来的植物物候变化，国内外学者通过直接地面物候观测、气候学数据以及地面卫星遥感资料开展了广泛的研究。但是在植物物候变化趋势及量化气候敏感性方面，仍然存在很大的不确定性和广泛争议。从而影响准确评价过去气候变化对植被的作用，影响可靠预测未来气候变化对植被生长的促进或制约。

本博士项目由瑞典国家科学研究委员会（FORMAS）资助（编号 2009-1124），旨在研究“气候变化对森林物候的影响以及对瑞典林业管理的预示”。我们通过建立近地面遥感观测塔网，采集分析地面遥感光谱资料，进行地面遥感观测理论研究，以及可靠易行的遥感光学传感器现场标定方法，提高近地面遥感采集的植被反射系数可靠性和准确度，以便用近地面遥感观测采集的植被季节性生长曲线，对卫星植被遥感资料进行评价和校正。我们研究发现，近地面遥感观测所采集的植被数据点，在传感器所覆盖的范围内呈柯西分布，意味着靠近观测塔的植被对观测信号影响最大。但是由于光学传感器的方向特性，最大影响点偏向传感器的观测中心。这一发现有助于正确设置地面观测塔，更有针对性的观测植被，减少非植被对近地面遥感数据的干扰。我们发现，如果采用我们提出的现场标定方法，观测结果甚至比传感器厂家的实验室标定还要准确。

现有的遥感植被指数，例如 NDVI，通过归一化方法降低传统的卫星传感器观测噪音及几何光学偏差，浪费了基于现代卫星传感器及算法优越性的更准确的植被反射率数据资料，不能正确反映北方常绿针叶林的季节性生长曲线，而是更多反映了这些地区降雪和融雪的季节特征。鉴于此，我们基于辐射传输方程，提出了新的植被指数—植物物候指数（PPI）。我们测试发现，PPI 跟树冠绿色叶面指数呈线性关系，跟碳通量（GPP）的相关性优于其它植被指数，并且 PPI 能够最大限度的降低季节性降雪融雪对重建植物物候的干扰作用，有助于提高北方常绿针叶林的物候重建准确性。

我们利用经几何校正的 MODIS 卫星遥感植被反射系数数据（NBAR），计算 PPI，重建北欧地区 2000-2014 年间的植物物候，计算 15 年内物候变化趋势，以及物候指标的气温、降雨等气候敏感性，和大气环流（北大西洋涛动和北极涛动）的相关性。本研究结果有助于提高近地面遥感植被观测的可靠性，减少在遥感植物物候重建和气候敏感性评价方面的不确定性。

Contents

1. Introduction

Phenology is the study of climate-dependent periodical phenomena of plants and animals (Abbe, 1905), and it particularly focuses on the timing, causes and inter relations of these phenomena (Lieth, 1974). The first phenology record might be "*Xia Xiao Zheng*", the Small Calendar for Xia Dynasty of China (ca. 2070 – ca. 1600 BC), in which mean monthly phenological events of plants and animals were inscribed on oracle bones. Later it was the polymathic giants Conrad Gessner, Ulisse Aldrovandi, and Carl Linnaeus who laid the foundations of mordern phenology study (Woolfson, 2013). In the era of Earth observation satellites and worldwide internet connections, particularly with the freely availabe satellite imagery (Wulder and Coops, 2014) and volunatry observations by enthusiastic nature lovers, phenology has regained accellerated interests for studying climate change impacts.

1.1 Plant phenology, why it is important

Plant phenology exerts major influences on carbon, water and energy exchanges between atmosphere and ecosystems, provides feedbacks to climate by altering leaf area index and consequently land surface albedo, canopy evapotranspiration, heat flux, and other biophysical properties, and affects the synchronized seasonal activities and differentiated niches of animals and consequently ecosystem functioning and services (IPCC, 2014; Pau et al., 2011; Tømmervik et al., 2009; Parmesan, 2007; Visser and Both, 2005; Walther et al., 2002; Keeling et al., 1996).

Based on satellite data, ground observations, and climatology records, many studies have revealed an advancement of spring and extension of growing season in the Northern Hemisphere and elsewhere during the recent past (Table A1 in Appendix). Such plant phenology changes are considered as detectable climate fingerprint (Parmesan and Yohe, 2003). The increased plant growth activities with warming and the extension of growing seasons will most likely result in higher sequestration of atmospheric carbon (Keenan and Richardson, 2015; Richardson et al., 2009). The decrease of atmospheric carbon will lead to reduced greenhouse effect — a negative feedback to global warming. Meanwhile, accompanying the

extension of growing season is the shortening of freezing season and less snow cover at northern latitudes. Consequently, the reduced albedo by vegetative surface will result in more absorbed solar energy to heat the land surface, and thus more water vapor from evapotranspiration to enhance the greenhouse effect — a positive feedback to global warming. Studies on plant phenology will improve the understanding of the interactions between climate and plant phenology.

Boreal forests store 32% of the world forest carbon (Pan et al., 2011) and the Eurasian boreal forests were estimated to be a continuous carbon sink over the past decades. Phenology variation will determine whether boreal forests become sinks or sources of carbon. In addition, plant phenology, in the aspects of seasonal tree growth and production, has economic implications for forest industry. In Northern Europe and particularly in Sweden, boreal forests have great economic importance with the forest industry accounting for more than 20% of industrial employment. The Swedish exports in forest industry in 2013 were valued at SEK 120 billion (Skogs Industrierna, 2013), with particularly increased exports to China. Understanding climate-induced phenology trends and the affected forest production may provide implications for forestry management and market strategy.

Climate change has resulted in a phenology shift in the time domain, and a range shift in the spatial domain (IPCC, 2014). Such shifts reflect species plasticity to environment change, but non-changed species might be at risk (Visser and Both, 2005). Plants provides primary production and habitats for animals, and the accurate estimation of past phenology variations is important for studying the phenology interactions between plants and animals, which have important socio-economic implications. For example, understanding of forest phenology is useful for pollen forecast (Karlsen et al., 2009a), and crop phenology for pest control (Jönsson et al., 2013).

1.2 Plant phenology, why it needs this study

Great efforts have been spent in retrieving plant phenology over past decades at regional, continental and global scales through ground phenology observations, climatological records, and remote sensing methods (see Table A1 of Appendix for the recent studies on plant phenology and trend estimation), yet there are still large uncertainties and disputations in phenology mapping, trend estimation, and climate sensitivities of plant phenology, which prevents reliable evaluations and projections of climate change impacts on plant phenology. This is particularly the case for northern latitudes of boreal forests which play an important role in sequestration of atmospheric carbon, but have insufficient ground phenology observations and poor remote sensing conditions.

At European northern latitudes, several studies have reported phenology variations over past decades using the Advanced Very High Resolution Radiometer (AVHRR) Global Inventory Modeling and Mapping Studies (GIMMS) dataset (e.g. Høgda et al., 2013; Karlsen et al., 2009b; Karlsen et al., 2007). It is however reported over west central Europe that the phenology derived from such dataset was inconsistent with ground manual observations for the period 2000-2011 (Fu et al., 2014). The phenology derived from the GIMMS dataset also disagreed with the results from other satellites observations (Wang et al., 2015). There are so far insufficient phenology studies over the Northern European region, both from ground manual observations and satellite remote sensing, compared with central European countries like Germany.

One way to address uncertainties in satellite remote sensing phenology and to reconcile the discrepancies in results from different methods is to zoom in on the satellite-viewing target both spatially and temporally at a fine resolution via using ground spectral towers. Ground spectral tower sampling of vegetation biophysical properties has been used to link satellite observation with *in situ* measurements of vegetation processes, such as plant phenology and productivity (Balzarolo et al., 2011; Eklundh et al., 2011). Such measurements are conducted continuously for several years at high temporal sampling interval at fixed locations. The benefits of ground spectral sampling are manifold: i) to validate and calibrate satellite-derived vegetation biophysical products, such as land surface albedo, Leaf Area Index (LAI), Fraction of absorbed Photosynthetically Active Radiation by plant canopy (FPAR) (Fensholt et al., 2004), ii) to upscale ground measurements of carbon fluxes to regional or global scales with the aid of satellite observations, and iii) to provide vegetation spectral information to help validating satellite derived gross primary production (Sjöström et al., 2013; Schubert et al., 2012). The ground spectral towers use light sensors with either nadir or off-nadir viewing to measure reflected radiation, yet how plants within the sensor viewing footprint contribute to the measured signals, and necessary *in situ* calibrations by users are often overlooked, leading to further great uncertainties in ground spectral sampling of vegetation.

Another way to reduce the uncertainties in remote sensing phenology is to use an appropriate method to retrieve plant canopy growth processes from satellite measurements, particularly over boreal forests that are dominated by evergreen conifers. The difficulties in retrieving plant phenology of coniferous boreal forests are manifold. One is that the optical remote sensing is often contaminated by clouds, resulting in frequent missing data. Another is the snow influence, and due to which, the retrieved phenology from Normalized Difference Vegetation Index (NDVI, Tucker, 1979; Rouse et al., 1973), for example, mainly reflected seasonality of snow activity, rather than coniferous canopy growth (Jönsson et al., 2010; Delbart et al., 2005). Furthermore, weak signals also lead to unreliable and noisy time series, particularly during phenophase transition time. These difficulties

call for new methods for improved phenology retrieval for boreal forests at northern latitudes.

1.3 What is done in this study

Four tasks were undertaken in this thesis:

i) Developing the measurement theory of ground spectral sampling for the established optical sensor network (Paper I);

ii) Developing the method of *in situ* calibration of multispectral sensors for reliable long-term sampling of vegetation (Paper II);

iii) Developing a new algorithm for improved phenology retrieval, to address the problems encountered in remote sensing phenology over boreal evergreen needleleaf forests (Paper III).

iv) Retrieving the plant phenology at European northern latitudes (> 50ºN) for the period 2000-2014, estimating phenology trends and the climate sensitivities, and exploring the relationships with atmospheric circulation patterns (Paper IV).

1.3.1 Ground spectral sampling

For the established ground spectral sampling sensor network, currently consisting of six sites in the study area (Figure 1), we investigated by modelling how the sensor viewing targets contribute to the measured signal. Such knowledge is particularly useful for targets with heterogeneous covers, such as mixed wet and dry areas, tree canopies with understory gaps and bare soil, and vegetation of different types. We found that the ground spectral sampling points follow a Cauchy distribution (Paper I). With Monte Carlo random sampling from the Cauchy distribution, the Hemispherical-Conical Reflectance Factor (HCRF) can be modelled from a bidirectional reflectance distribution function (BRDF). The HCRF modelling result can be used in the design of ground spectral towers, with respect to tower height, viewing direction, and oblique viewing angle; to minimize the BRDF effects on measurements and to make the measurement best reflect the target vegetation. For the situation of downward-looking sensors with hemispherical view, we analyzed the tower influence on the measured signals, so as to properly design the tower and minimize the tower influences. The hemispherical-view sensors are often used in measuring of Photosynthetically Active Radiation (PAR).

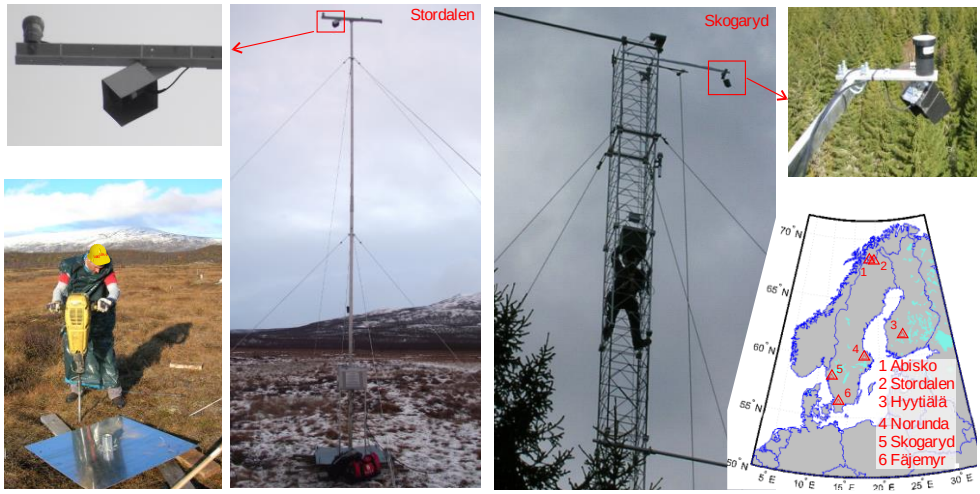

Figure 1. Ground spectral tower sampling of vegetation at Stordalen mire and Skogaryd spruce forest. The downward-looking sensor views the ground obliquely. Left photo: Preparing tower foundation by Dr. Schubert. Right map: six ground tower sites in this study area.

1.3.2 Light sensor calibration

We explored and analyzed methods of calibrating light sensors that can be easily carried out by users at measurement sites (Figure 2). Regular sensor calibration is essential for reliable measurements, but sending sensors back to manufacturers or professional laboratories for calibration is time-consuming, expensive, and disrupts measurements by delivering sensors back and forth. For vegetation reflectance measurement, the sensor can be calibrated against a diffuse white reflectance reference panel, e.g. a white Spectralon panel. We devised the calibration procedure and analyzed the uncertainty propagation from calibration to measured reflectance and vegetation index. The proposed field calibration method will improve the reliability of long-term spectral measurements of vegetation. Such accurate vegetation reflectance values can then be used in physically-based vegetation indices for better characterizing vegetation growth processes.

1.3.3 Physically-based vegetation index PPI

Based on the Hapke (1993)'s diffusive reflectance theory, we proposed a plant phenology vegetation index (PPI). The PPI is computed from BRDF-adjusted red and near infrared reflectance measured either from ground spectral towers or from satellites. The PPI formulation takes full advantage of sophisticated algorithms for estimating standardized reflectance with reduced angular influences, as well as

improved vegetation reflectance measurements by ground spectral towers. From our derivation, PPI is linearly related with green LAI in theory, and thus there is no saturation in dense canopies. We tested PPI against measured canopy LAI from the network of global validation sites. To assess the potential of PPI for monitoring plant canopy growth, we compared PPI time series with flux tower estimated gross primary productivity (GPP) curves, and manual observations of phenology status of trees. We also analyzed influences of the snow and soil brightness on PPI. Results from these primary tests and analyses demonstrated the potential of PPI to address the problems of remote sensing phenology encountered in boreal coniferous forests.

Figure 2. Calibration of multispectral sensors at Stordalen mire, Hyytiälä pine forest, Norunda forest clearcut, and Lund (INES department roof).

1.3.4 Plant phenology at European northern latitudes 2000-2014

We used PPI to retrieve plant phenology from the Moderate-resolution Imaging Spectroradiometer (MODIS) nadir BRDF-adjusted reflectance (NBAR) at European northern latitudes for the period 2000-2014. We estimated the trend of start of growing season (SOS), end of growing season (EOS), length of growing season (LOS), and the PPI integral during the time span. The PPI integral is regarded as a measure of plant production of the growing season. We analyzed the temperature and precipitation sensitivities of these phenology metrics, and their relationship with the North Atlantic Oscillation (NAO) and the Arctic Oscillation (AO).

1.4 Objectives

This thesis is a part of the program "*Climate change impacts on forest phenology, and implications for Swedish forest management*" funded by the Swedish Research Council *Formas* (PI L. Eklundh). The aim of the program is to estimate climate change impacts on Swedish forests and its socio-economic implications. Within this broader program aim, this thesis has three specific objectives:

i) Developing remote sensing methods for improved phenology retrieval over large areas.

ii) Mapping phenology changes in northern Europe.

iii) Evaluate climate influences on phenology over the region.

2. Material and methods

2.1 Data

2.1.1 Satellite data

The MODIS NBAR MCD43 product (Schaaf et al., 2002) was used in this thesis to derive Plant Phenology Index (PPI), and then to retrieve phenology metrics, including SOS, EOS, LOS, and the PPI integral. The MODIS NBAR is the land surface reflectance at sensor nadir-view with the sun at local noon. It is computed at a nominal 500 m spatial resolution for every 8-day interval from continuous 16-day observations by both Terra and Aqua satellites (Schaaf et al., 2002; Strahler et al., 1999). We also used other MODIS products: MOD09A1/MYD09A1 8-day 500m land surface reflectance for the comparison of tower NDVI measurements, and MOD15A2 8-day 1km LAI product for the comparison of PPI and ground measured LAI.

We tried several other satellite products for phenology retrieval, for example, the NDVI computed from MODIS MOD09GQ 250m daily land surface reflectance. The extreme noise in the daily time series (Figure 3) needs further processing, for example using maximum-value compositing technique (Holben, 1986), which has already been done in other MODIS land surface reflectance product, such as the 8-day reflectance data MOD09A1 that was used in Paper I for comparing with tower data. We also analyzed the vegetation optical depth (VOD) data derived from passive microwave remote sensing (Jones et al., 2011). Figure 4 shows VOD time series for four flux tower sites in Sweden and Finland. These VOD temporal profiles show a pattern counter-intuitive to the vegetation growth process of single growing seasons in the Nordic region, plus long periods of missing data in wintertime, which implies that further studies and processing of VOD data to overcome surface water influences is necessary. Based on these primary tests, we did not use MODIS daily data nor microwave remote sensing VOD data; instead we used the 8-day 500m NBAR data for remote sensing phenology retrieval over Northern European regions.

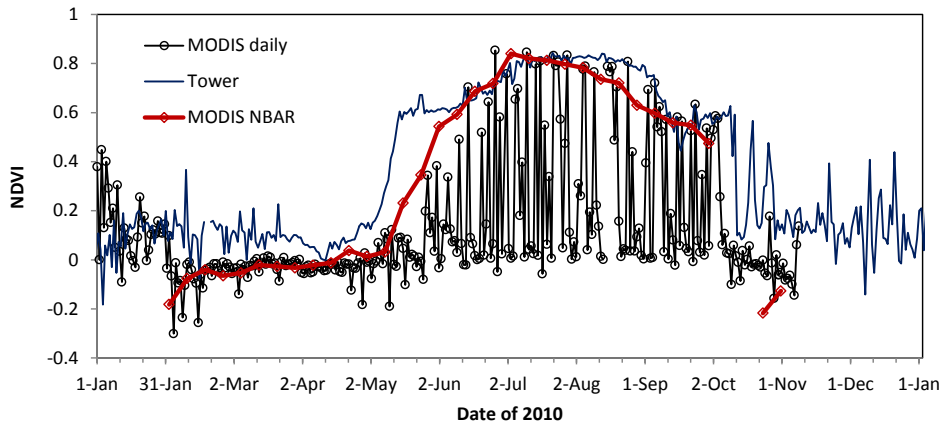

Figure 3. The NDVI time series calculated from ground tower measurement, MODIS daily data (MOD09GQ), and MODIS NBAR data (MCD43A2) in 2010. Notice the noise in MODIS daily data. MODIS data are from the signal pixel that the tower located.

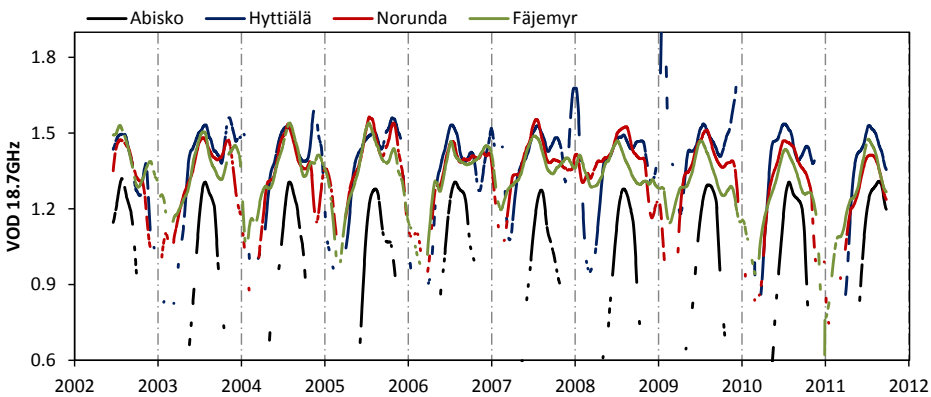

Figure 4. VOD time series from AMSER-E for four ground sites in Sweden and Finland. Data from Jones and Kimball (2011).

For analyzing MODIS data for a specific site, such as a ground spectral tower site, a flux tower site, or an LAI validation site, I developed a modisGrid2KML tool to generate MODIS pixel for checking the site location and land cover in Google Earth (Figure 5). The tool is freely downloadable at http://www.mathworks.com/matlabcentral/fileexchange/34891. When the target vegetation observed at the site was not representative of the landcover in the MODIS pixel, a nearby proper pixel was used instead to compare the results from MODIS with ground observations. If it is not mentioned in the thesis that the average value of pixels with same land cover type was used, we used the MODIS data of a single pixel to compare with ground spectral measurements (Paper I) and

ground phenology (paper IV) so as to avoid using the mean pixel values of different land covers.

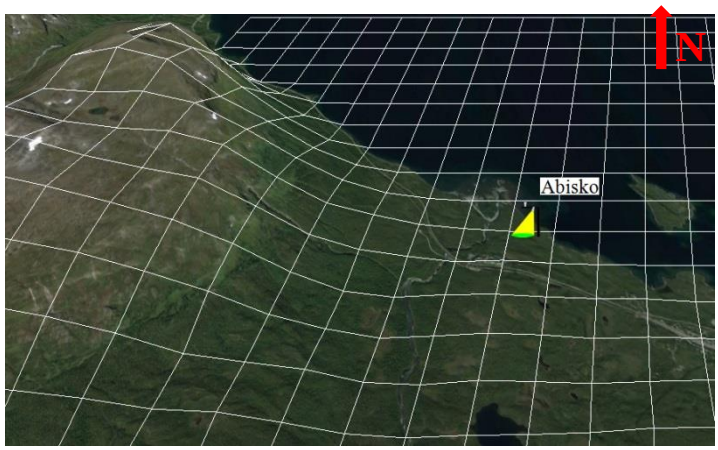

Figure 5. MODIS Sinusoidal tile grid (500m cellsize) at the ground spectral tower site of Abisko forest, northern Sweden. The MODIS pixel in which the tower is located covers a small portion of water, which implies that extra caution is needed when considering the point spread functions of MODIS sensors.

2.1.2 Ground data

Various ground data are used in this thesis to demonstrate ground spectral tower sampling of vegetation, and to validate and evaluate satellite-derived PPI and phenology metrics.

Ground spectral data

Continuously measured NDVI in 2010 at five ground spectral towers were demonstrated in Paper I, in comparison with MODIS observed NDVI. The NDVI measurement was conducted using two sensors mounted above the plant canopies: one measuring hemispherical irradiance and the other measuring reflected directional radiance from the top of canopy, from which reflectance was calculated. Then NDVI was estimated from red and NIR reflectance: $NDVI = (NIR - red)/(NIR + red)$. These reflectance data were calculated by using manufacturer calibrations.

In Paper I, we also showed continuously measured canopy FPAR using four-sensor observations (Figure 6b) at Abisko forest spectral tower site, and three-sensor observations at Norunda site. For measuring PAR transmission through canopy, a matrix of separated sensors was used, composing 14 sensors in Norunda and 4 sensors in Abisko. The averaged transmittance was used for estimating

FPAR to reduce bias from canopy non-uniformity (clumping). The sensor for measuring ground PAR reflectance was omitted at Norunda site due to the weak ground reflection signal.

Another type of ground spectral measurements was used in Paper III to test PPI in relation with LAI. We measured red and NIR reflectance on stacked leaves with the downward-looking sensor pointing at nadir direction (Figure 6a). The stacked-leaf experiment was used to compute vegetation indices NDVI, EVI (Huete et al., 2002) and PPI for testing their relationships with the number of leaf layers (LAI). In the experiment, the sensor pair was calibrated using the method developed in Paper II.

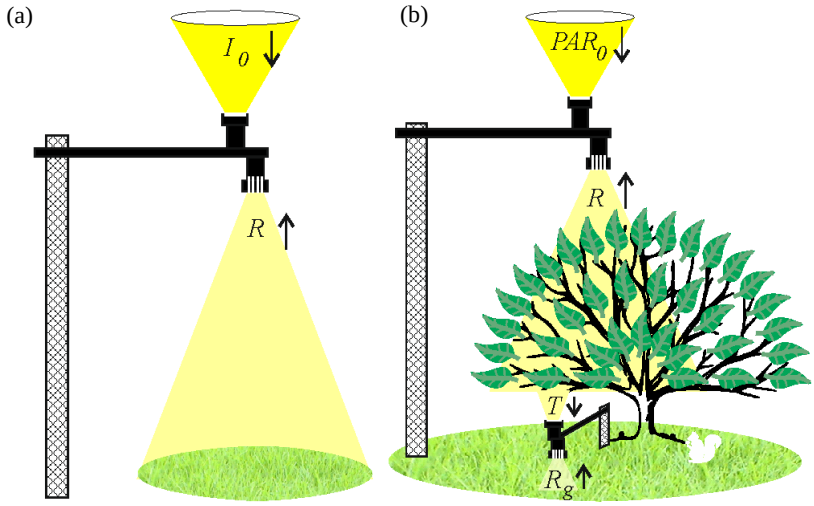

Figure 6. Illustration of ground-based spectral measurement. Arrows indicate the direction of radiant flux measured. (a) Applicable for narrow band multispectral sensor or PAR sensor. (b) FPAR measurement for forest canopy. Note that the radiant flux cones are only for illustration purpose. The upward-looking sensor is always with a hemispherical view for measuring irradiance. The downward looking sensor has either conical or hemispherical view for a multispectral sensor, and always hemispherical view for a PAR sensor. Usually a sensor matrix is used for measuring averaged transmittance T to reduce bias by canopy clumping.

Manual phenology observations

We used manual phenology observations from six sites in Sweden, and the observations were continuously conducted by the Swedish University of Agriculture Sciences (SLU) and the Abisko Scientific Research Station. The manual phenology observations by SLU are carried out on several representative trees, and the average date of each first event was used to compare with PPI phenology.

Manual autumn phenology observations by citizen science in 2013 throughout Sweden were used to compare with PPI derived autumn phenology.

Almost 12,000 reports of autumn leaves on more than 2,000 trees from 378 different locations in the country were collected. Considering the nature of citizen science, we did not compare these autumn events with PPI phenology point-by-point; instead we compared their latitudinal profiles (Paper IV).

Flux-tower derived GPP

GPP estimates from Flux-tower data at 19 sites in Northern Europe were used to evaluate PPI derived phenology. The data were collected from FLUXNET (www.fluxdata.org) and colleagues. The GPP temporal profiles of three sites were correlated to PPI in Paper III, and the GPP-derived phenology metrics (SOS, EOS, LOS, and the GPP integral) of 18 sites were used to evaluate PPI derived phenology metrics in Paper IV.

Radiation-based LAI measurements

We collected reference LAI measurements from BELMANIP biophysical variable validation network (Garrigues et al., 2008; Baret et al., 2006; Morisette et al., 2006), FLUXNET (ORNL DAAC, 2013), the European VALERI project (Baret et al., 2006), and other sources. Since the red and NIR reflectance derived PPI reflects green LAI, and the radiation-based LAI estimates are from canopy gap fractions and are influenced by all canopy elements that can block the blue light beams measured by the LAI instrument (LI-COR, 2009), the radiation-based LAI data at the leaf-yellowing phase of two deciduous broadleaf forest (DBF) FLUXNET sites were not used in the analysis in Paper III.

2.1.3 Climate data

Gridded mean daily temperature and precipitation data (E-OBS, version 10.0, Haylock et al., 2008) were used in Paper IV to estimate phenology climate sensitivities. The monthly atmospheric circulation data of NAO and AO indices were downloaded from http://www.cpc.ncep.noaa.gov, and the PPI derived phenology were correlated to these atmospheric circulation patterns. An example of these time series of climate data and atmospheric circulation indices over Skåne is shown in Figure 8, presenting an overview of how climate varied in the 2000s, in comparison with the preceding five decades, together with the decadal influences of atmospheric circulation patterns.

Regarding SOS and EOS, the mean temperature within the three months of the onset date (the month of mean SOS or EOS and the preceding two months) was used in temperature sensitivity estimation. The annual mean temperature was used to estimate LOS and the PPI integral temperature sensitivity. As to precipitation, the total precipitation of the corresponding periods was used in sensitivity estimations. The mean atmospheric circulation index of the

corresponding periods was used to Spearman correlation coefficients with these phenology metrics for the period 2000-2014.

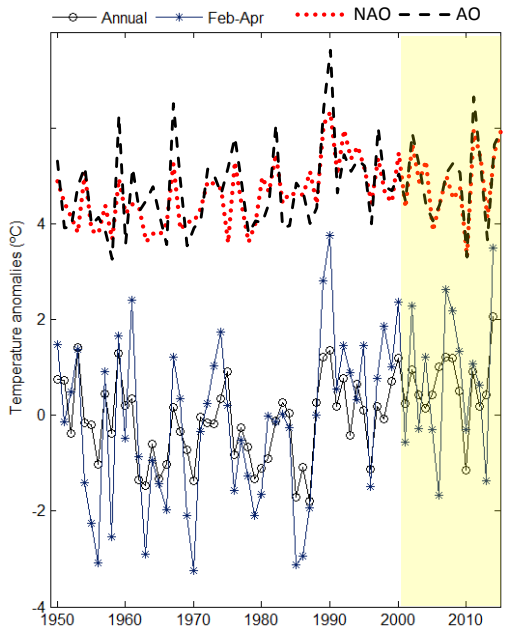

Figure 8. Annual and February-to-April mean temperature anomalies in Skåne, southern Sweden for the period 1950-2014 from E-OBS gridded climate dataset, together with mothly NAO and AO indices averaged over the period February to April. Shaded area indicates the study period 2000-2014 in this thesis.

2.2 Mathematical derivation

The derivation of joint Cauchy distribution of ground sampling points is presented in Appendix A2.1, with a Matlab GUI simulation of sensor footprint, freely downloadable at http://www.mathworks.com/matlabcentral/fileexchange/35503. In Paper I, we only gave marginal Cauchy distributions along the x-axis and the y-axis separately.

We derived formulae to estimate the tower influences (tower shade and sensor view blocked by the tower) on the hemispherical downward-looking sensor, such as a PAR sensor, shown in Appendix A2.2. In A2.3 we show the derivation of standard uncertainty of the NDVI inherited from the uncertainty of the reflectance measurements. Other derivations, like the PPI formula (Paper III), and

fractions of PAR components from measurements (Paper I), are clear in the papers and not repeated here.

2.3 PPI calculation

PPI is calculated as

$$PPI = -K \times \ln\left(\frac{(NIR-red)_{\max}-(NIR-red)}{(NIR-red)_{\max}-(NIR-red)_{Soil}}\right), \quad (1)$$

where *NIR* and *red* are nadir-viewing reflectance in red and NIR spectra. The $(NIR\text{-}red)_{max}$ is the maximum difference between NIR and red for a specific site from many years of measurement. Figure 7a shows a map of $(NIR\text{-}red)_{max}$ from MODIS NBAR dataset for the years 2000-2014 and it closely resembles the CORINE land cover map (EEA, 2007) in Figure 7b. The $(NIR\text{-}red)_{Soil}$ is the difference between NIR and red for soil, and an empirical value of 0.09 (see Paper III) was used here. The gain factor *K* is a function of the sun zenith angle, the *G* function of leaf angular distribution, and instantaneous diffuse fraction *dc* of solar radiation:

$$K = \frac{0.25 \cdot \cos(\theta)}{(1-d_c)\cdot G + d_c \cdot \cos(\theta)} \cdot \frac{1+(NIR-red)_{\max}}{1-(NIR-red)_{\max}}. \quad (2)$$

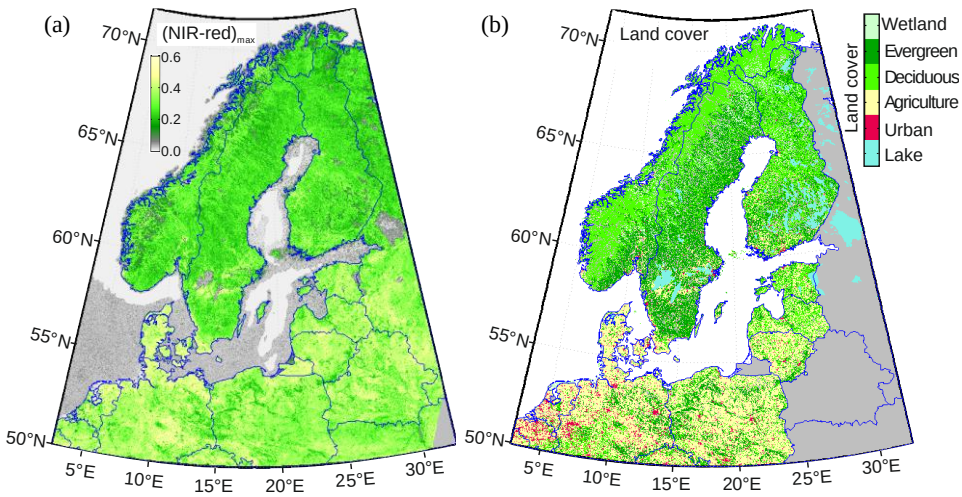

Figure 7. The map of a) $(NIR\text{-}red)_{max}$ closely resembles the map of b) CONRINE land cover.

We used G = 0.5 for spherical leaf distribution for either flat leaf (Ross, 1981) or needle leaf (Stenberg, 2006). The instantaneous diffuse fraction was estimated as $d_c = 0.0336 + 0.0477m(\theta)$ for standard atmosphere following

(Suehrcke and McCormick, 1988). The air mass $m(\theta)$ in relation with solar zenith angle was computed as $1/\cos(\theta)$ for $\theta < 80^\circ$, and $0.4281 \times e^{0.0307\theta} + 2.693 \times 10^{-14} \times e^{0.3848\theta}$ for $\theta \geq 80^\circ$, based on the ISO standard air mass table by Kasten and Young (1989). The fitting equation for θ>80º was obtained from Matlab.

2.4 Phenology retrieval using TIMESAT

2.4.1 Parallel TIMESAT

TIMESAT is a program developed by P. Jönsson and L. Eklundh for analyzing time-series of satellite sensor data (Jönsson and Eklundh, 2004; Jönsson and Eklundh, 2002). The program has been undergone continuous improvement and used extensively for time series of satellite data processing and phenology retrieval (e.g. Jamali et al., 2015; O'Connor et al., 2012; Schubert et al., 2012; Sjöström et al., 2009; Olofsson and Eklundh, 2007). Among the advantages of TIMESAT, one is its capability to efficiently process large quantity of time-series image data using sophisticated fitting algorithms to retrieve phenology metrics. This capability is further enhanced by using parallel computing with OpenMP, an interface for shared memory parallel programming (Chapman et al., 2008). Parallel I/O is one of the tricky processes in OpenMP. The flexible output file format of TIMESAT made the parallel writing easier, but the parallel reading had to be treated with caution in order to avoid a data race condition — the situation when more than one threads may concurrently access the same shared variable without holding any common locks and with at least one thread modifying the variable (Chapman et al., 2008). When a chunk of data was read in to the computer memory, it was dynamically divided into smaller chunks and scheduled to all available processors on the computer. The analysis used 24 processors, and reduced the processing time from two weeks to one day for all 15 years of 6 tiles of MODIS data (100GB in total).

2.4.2 Phenology retrieval

Various methods were tested for phenology retrieval, including

- derivative methods: the first derivative - the maximum slope, the second derivative - the maximum change rate in slope, and the third derivative - the maximum change rate in time series curvature during phenology transition (Zhang et al., 2003);

- threshold methods: a fixed vegetation index value, a fixed relative percentage of individual year's amplitude (Jönsson and Eklundh, 2004; Jönsson and Eklundh, 2002), and a fixed relative percentage of mean amplitude for all years;
- forward-backward moving average (Reed et al., 1994); and
- other methods used in time series classification, such as time series similarity by an Euclidean distance measure, and dynamic time warping (Ratanamahatana and Keogh, 2004).

Considering that the developed method had to be operational with large amounts of image data, and that the PPI has a linear relationship with LAI, we finally selected the threshold method with a relative percentage of mean amplitude. We set the threshold at 20% of the mean amplitude for all years of a site (Paper IV). The SOS and EOS were defined as

$$SOS = \underset{DOY}{\arg\min}(PPI_{DOY} > 20\% \times meanPPI_{Amplitude} + meanPPI_{BaseLevel}), \quad (3)$$

$$EOS = \underset{DOY}{\arg\max}(PPI_{DOY} < 20\% \times meanPPI_{Amplitude} + meanPPI_{BaseLevel}). \quad (4)$$

The settings are visualized in Figure 9 using the TIMESAT GUI interface.

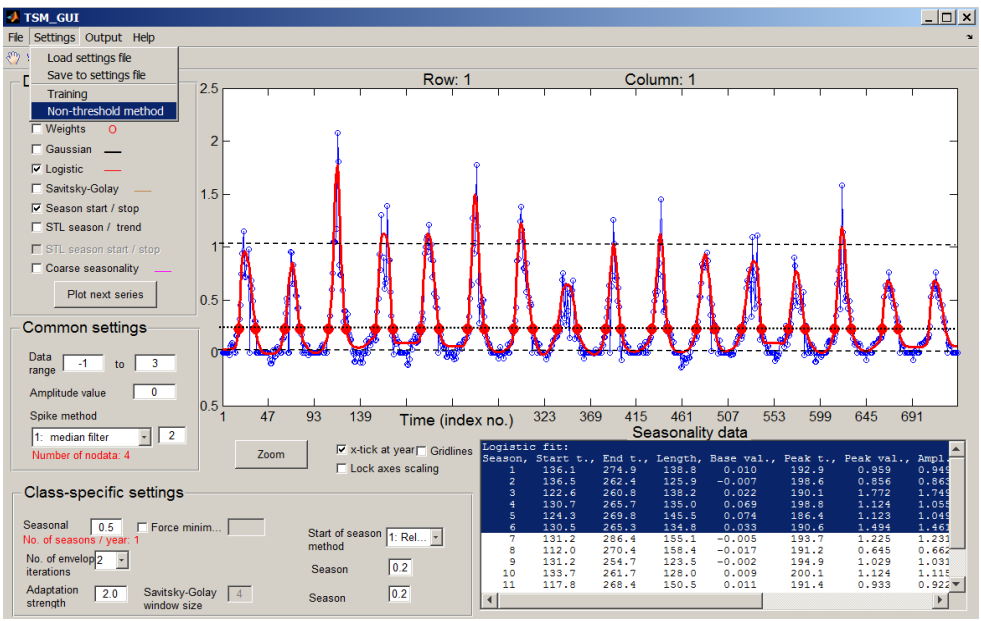

Figure 9. Using TIMESAT to retrieve phenology metrics from a threshold of 20% mean PPI amplitude.

2.5 Data analyses

2.5.1 Multivariate vs. univariate

We used both multivariate regression and univariate regression, both simple correlation and partial correlation to explore the relationship between phenology and climate variables. It turned out that multivariate regression could give a higher R^2 than from univariate regression, but that the resulting more complicated spatial patterns needed further exploration as to the interrelationships among the climate variables. We did not include the multivariate regression and partial correlation in Paper IV because we were not aiming an optimal phenological model regarding R^2. We simply explored the relationship between phenology metrics and temperature or precipitation, despite the relationships between temperature change and snowfall, rainfall, or other local effects.

2.5.2 Panel data analysis

We used a panel data analysis method (Hsiao, 2003) to estimate phenology trends and climate sensitivities at European northern latitudes for the period 2000-2014. Panel data analysis has advantages over pixel-by-pixel methods by overcoming problems hampering reliable and significant trend or sensitivity estimates caused by short time series of insufficient data, frequent noise, and missing data that hamper reliable and significant trend or sensitivity estimates. We applied the method by using grid cells from the gridded E-OBS climate dataset as non-overlapping panels, and used fixed-effect ordinary linear regression (OLS) to estimate phenology trends and sensitivities β:

$$y_{i,t} = \beta \cdot x_t + \alpha_i + \varepsilon_{i,t}\,, \tag{5}$$

where $y_{i,t}$ is the phenology metric (SOS, EOS, LOS, or the PPI integral) at MODIS pixel i within the panel for year t (t = 2000 to 2014). x_t is the climate variable (temperature or precipitation) in the sensitivity estimation, and $x_t = t$ in the trend estimation. Thus β is either a sensitivity estimate of the climate variable or phenology trend for the time variable. $\varepsilon_{i,t}$ is a random error in OLS at MODIS pixel i and year t. α_i is an unobservable fixed-effect and assumed to be independent of t. α_i disappears when using the anomalies (the difference between a variable and its temporal mean value) of dependent and independent variables:

$$(y_{i,t} - \overline{y_{i,t}}) = \beta \cdot (x_t - \overline{x_t}) + \varepsilon_{i,t}\,. \tag{6}$$

Therefore α_i has no influence on the regression slope β, and it only influences the intercept of each MODIS pixel in the OLS.

Each panel (~25 km cell size of E-OBS grid) covered ca. 2500 MODIS pixels (500 m cell size). The actual number range can be up to over 3000, depending on

latitudinal location and proportion of vegetation cover in the panel. Panels with less than 20 valid MODIS pixels were discarded from further analysis. For the panel data of dependent phenology variables and independent climate variables, we also estimated their Spearman correlation coefficients. The panel data analyses resulted in statistically significant estimates over most parts of the study area, with about 90% of all grid cells significant at p =0.01.

2.5.3 Mann-Kendall trend analysis and Theil-Sen slope estimator

Besides panel analysis, we used robust nonparametric methods, Mann-Kendall trend analysis (Mann and Whitney, 1947) and Theil-Sen slope estimator (Sen, 1968; Theil, 1950), to analyze trends of deseasonalized short time-series and estimate their slopes. This was done pixel by pixel. Although most results were insignificant (p > 0.05), they provided robust estimates to cross-check the significant slopes estimated from the panel analysis.

The ranked correlation of Mann-Kendall τ is calculated as

$$\tau = \frac{S}{n(n-1)/2}, \text{ and } S = \sum_{t1=2000}^{2013} \sum_{t2=t1+1}^{2014} \text{sgn}\left[(y_{t2} - y_{t1})(x_{t2} - x_{t1})\right], \quad (7)$$

where y is the phenology metric of a MODIS pixel, and x is, in sensitivity analysis, the climate variable of a grid cell in which the pixel is located, or time in trend analysis. *t1* and *t2* are the years 2000 to 2014. The sgn(·) is a sign function, with 1 for a positive number, 0 for 0, and -1 for a negative number. The tied (same value) observations were not treated here.

The Theil-Sen slope β (either trend or sensitivity) was estimated as the median slope of all $n(n\text{-}1)/2$ combinations:

$$\beta = \underset{t2>t1}{median}\left[(y_{t2} - y_{t1})/(x_{t2} - x_{t1})\right] \quad (8)$$

.

The significance test for the trend was done by calculating z-score:

$$Z = \frac{S - \text{sgn}(S)}{\sqrt{n(n-1)(2n+5)/18}}, \quad (9)$$

where n is the number of years (15 years in this study). The p-value was then found for the standard normal distribution $N(0,1)$ given a Z-score.

3. Results and discussion

3.1 Ground spectral tower sampling of vegetation reflectance (Paper I)

3.1.1 Spectral sensor footprint

Given a sensor with a field-of-view (FOV) of β viewing at the ground with an off-nadir angle α at a height H above the canopy, the sampling points (x,y) by the sensor follow a joint Cauchy distribution within the footprint ellipse:

$$f(x,y) = \frac{H}{2\pi\left[1-\cos(\alpha+\beta/2)\right]} \cdot \frac{1}{\left[(x-L)^2+y^2+H^2\right]^{3/2}}, \quad (10)$$

where $L = H \cdot \left[\tan(\alpha+\beta/2)+\tan(\alpha-\beta/2)\right]/2$. The ellipse has a geometric dimension:

Semi-major axis:

$$a = H \cdot \left[\tan(\alpha+\beta/2)-\tan(\alpha-\beta/2)\right]/2, \quad (11)$$

and semi-minor axis:

$$b = H \cdot \left\{\left[\cos(\alpha)+\sin(\alpha)\cdot L/H\right]^2/\cos^2(\beta/2)-L^2/H^2-1\right\}^{1/2}. \quad (12)$$

Hence the spectral sensor viewing area is πab. The distance from the closest viewing point to the mast is $D = H \cdot \tan(\alpha-\beta/2)$.

By sampling the Cauchy distribution, the ground spectral points are illustrated in Figure 10 using the aforementioned footprint tool for a spectral sensor. A 60º-FOV sensor viewing at the ground with an off-nadir angle of 55º at a height of 8 m above the canopy (Paper I, the case of Abisko forest) will have an ellipse footprint of 88 by 28 m (major and minor axes). However, the vegetation in a distance of 25 m in the vicinity of the tower affects the measurement up to 85% of the signal, if the sensor has an ideal cosine (Lambertian) directional response. Considering that the actual sensor directional response is not Lambertian, the sampling target shifts toward the sensor focus (FOV center), covering an area of 15 by 8 m. Thus the ground spectral tower measures the vegetation growth activity and phenology phases mostly within this small region. Any other non-vegetation objects in this region, such as bare soil, water, and measurement facilities will

greatly bias the measurement results. For other spectral tower designs, the viewing area can be easily estimated using the footprint tool.

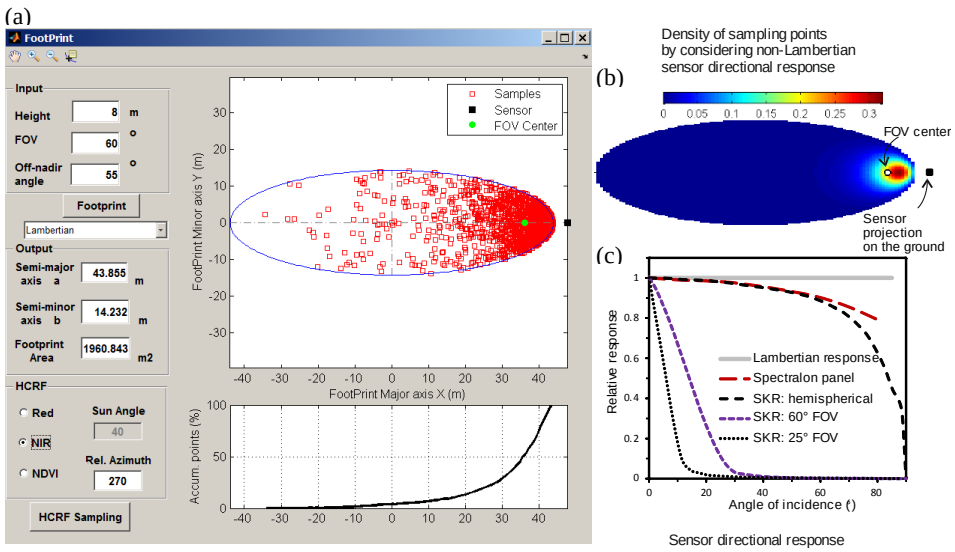

Figure 10. Spectral sensor footprint and the distribution of the sampling points (a). The measurement center shifts to the sensor FOV center (b), when using the actual sensor directional response function for 60º FOV sensor (c).

3.1.2 Tower influences

A downward-looking hemispherical view sensor presents a special case with α =0°, and β = 180°. Such a configuration is extensively used in PAR and net radiation measurements. From the footprint model of the Cauchy distribution, we calculated that 99% of the radiant flux sensed by such a downward-looking sensor comes from a circular area with a radius of 10H (H is the tower height). This calculation is in agreement with that given by Campbell Scientific Inc. for a CNR1 Net Radiometer (Campbell Scientific, 2011).

For the case of downward hemispherical view, the sensor will sense both the spectral tower and the tower shadow. The fraction of shadow in the footprint is (Appendix A2.2):

$$f_S = d/(10\pi H), \quad (13)$$

where d is the tower width, and H is the tower height. Comparatively, Campbell Scientific (2011) roughly estimated that the tower shadow influence is less than 1% for $d < 0.1H$. In the sensor's hemispherical view, the fraction of the sensor viewing solid angle blocked by the tower is

$$f_\Omega = d/(\pi l), \quad (14)$$

where *l* is the distance of the sensor to the tower (boom length). The recommended distance of the sensor to the tower by Campbell Scientific (2011) is at least 1 meter. About 3% of the view will be blocked for a sensor with one meter away from a tower mast of 0.1 m in diameter. Tower influences on the hemispherical view sensor can be reduced by painting the tower with matt black color, besides reducing tower width and increasing boom length if possible. The matt black color should also be used for the tower base, fastening strings and other similar items that are in the sensor view.

3.1.3 Measurements

Regarding the NDVI, the tower measurements and MODIS observations agreed with each other very well during the 2010 vegetation growing period at all five sites. Tower measurements showed more detailed NDVI variations at phenology transition periods, during which the NDVI was at a rather high level. These NDVI curves showed that NDVI was more sensitive to snow melting (NDVI had a large rapid increase within a short time) than to leaf emergence and elongation (NDVI gently increased for a period and then got saturated).

To exemplify how tower measurements can add be the interpretation of remotely sensed data from satellite, we here we show the ground spectral tower measurement results at the Abisko forest (Figure 11). The tower NDVI in Figure 11b showed that the NDVI levelled for a short while after the first abrupt increase caused by snow melting, and a moderate increase in NDVI happened again 18 days after the snow melting, which was linked to the onset of leafing.

Figure 11 also compares spectral tower measured FPAR with the MODIS FPAR product. We here measured pure canopy absorbed PAR by using the 4-sensor method. During the vegetation growth period, both of the FPAR estimates show seasonal variation, but the MODIS FPAR (0.66 on average) is overestimated by up to 50% during the peak growing season against tower FPAR (0.44). This is mostly due to that MODIS FPAR also includes the PAR absorbed by understorey vegetation, soil and litter. Fensholt et al. (2004) also reported that MODIS FPAR was overestimated by up to 20% in Africa semi-arid area of sparse vegetation cover. The overestimation of MODIS FPAR was also reported by Steinberg et al. (2006) in boreal forests of Alaska. In contrast, Majasalmi et al. (2015) reported that MODIS FPAR was 20% underestimated in a boreal forest of Finland during the peak season. Though interpretations from these few ground sampling points should be interpreted with caution, the disagreements between MODIS FPAR and ground measurements underline the necessity of further field validation and comparison of satellite derived FPAR products.

Besides for validating satellite products, the tower-measured temporal course of FPAR is useful for validating model-derived FPAR. For example, Majasalmi et

al. (2014) modelled FPAR from the leaf single-scattering albedo and the spectral-independent probability of photon re-collision within canopy (Knyazikhin et al., 2013) based on a simple forest albedo model proposed by Stenberg et al. (2013). Such a FPAR model based on very few measurable variables is more operational than other models using extensive forest inventory data, for example the canopy reflectance model by Kuusk (1995). Tower-based FPAR time series may provide unique data for validating an operational FPAR model.

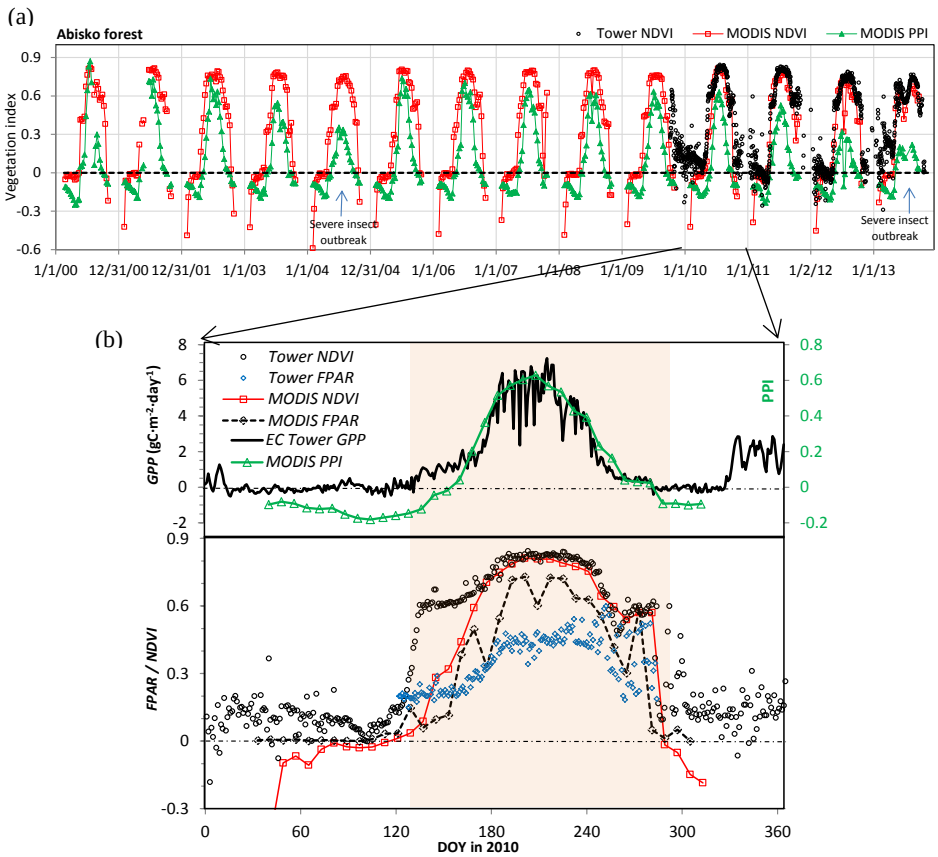

Figure 11. Spectral measurements at Abisko birch forest, Sweden. MODIS NDVI and PPI were computed from MODIS NBAR reflectance MCD43A2, MODIS FPAR is from MODIS LAI&FPAR product MCD15A2. MODIS data were averaged for several pixels with birch forest. See Section 3.3 for the description of MODIS PPI curve.

3.2 *In situ* light sensor calibration (Paper II)

When developing the sensor calibration procedure, we particularly paid attention to the uncertainty propagation from calibration. The uncertainty analysis here applies to all kinds of normalized difference spectral indices, such as NDVI, the photochemical reflectance index (PRI, Gamon et al., 1997), normalized difference water index (Gao, 1996) and etc that are measured by a pair of multispectral sensors.

Taking NDVI as an example, we can write the relative standard uncertainty in NDVI measurement that propagated from calibration as:

$$\frac{u(NDVI)}{NDVI} = \frac{1-NDVI^2}{2NDVI} \cdot \sqrt{(\frac{u(red)}{red})^2 + (\frac{u(NIR)}{NIR})^2} \quad (15)$$

where *u(NDVI)/NDVI* is the relative standard uncertainty in NDVI, *u(red)/red* and *u(NIR)/NIR* are relative reflectance uncertainties that are caused by calibration. In our calibration test, the reflectance uncertainty was estimated as 2% by following the proposed procedure, smaller than the 5% specified as the manufacturer calibration uncertainty. Thus the uer calibration can be more accurate than the manufacturer calibration. The NDVI uncertainty is dependent on NDVI levels (Figure 12) following Eq. (15). The measurements of high NDVI values (usually measured over dense vegetation) are more certain than low NDVI values (usually measured over sparse vegetation). That is, more cautions are needed to accurately measure NDVI over spare vegetation.

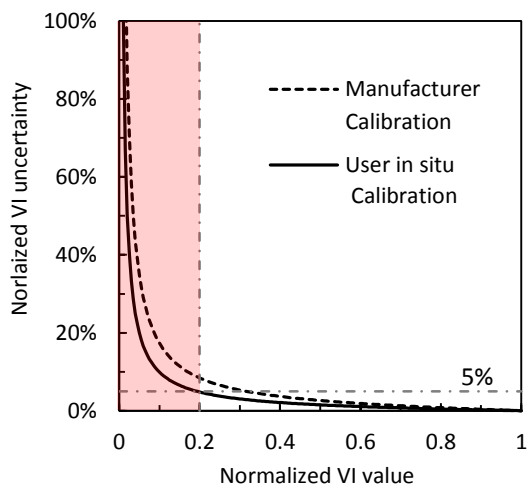

Figure 12. Uncertainties in measured normalized vegetation index (VI) in relation with VI magnitude. The curves are based on the reflectance uncertainty estimation from calibrations.

Eq. (15) and the uncertainty estimation are applicable to PRI, which is a normalized difference between reflectances in two green bands (wavelength 531 and 570 nm). The VI uncertainty in relation with the VI magnitude is shown in Figure 12.

Figure 12 shows that for a VI value larger than 0.3, its uncertainty is less than 5%. Therefore the NDVI estimates over non-sparse vegetation are generally reliable. For moderately sparse vegetation (VI is around 0.1-0.3), the user *in situ* calibration is preferred to manufacturer lab calibration. The PRI is usually measured with values less than 0.2 or even less than 0.1 (Harris et al., 2014; Gamon et al., 1997), which implies that extra caution is needed to reduce the calibration uncertainty, as well as uncertainties from other sources, in order to make PRI measurements accurate. Otherwise the high uncertainty in PRI will hamper reliable estimation of plant light use efficiency from PRI.

3.3 PPI (Paper III)

3.3.1 The Hapke's diffusive reflectance theory

The plant phenology index (PPI) was derived from the Hapke (1993)'s diffusive reflectance theory. Diffusive reflectance describes the incoming radiant energy being scattered backward to the original hemisphere after extinction within a medium. The widely used Kubelka–Munk reflectance (Kubelka and Munk, 1931) is a kind of diffusive reflectance, but the Kubelka-Munk theory has been criticized (e.g. Edström, 2010; Hapke, 1993) for several mistakes:

i) incorrect concept about light scattering in a medium. It wrongly assumed that scattering happens in the direction opposite to the light propagation, i.e. no forward scattering, and it also wrongly assumed that the scattering is independent of absorption;

ii) the light propagation over the upward and downward hemispheres results in a factor of ½ in the radiative transfer equation, which leads to a factor of 4 in the final solution. The Kubelka-Munk theory wrongly used a factor of 1 and resulted in a factor of 2 in the solution of exponential expression. This wrong factor of 2 is currently used in the vegetation remote sensing community (e.g. Campbell and Norman, 1998; Allen and Richardson, 1968), although it did not create errors in calculation due to other adjustable factors.

The Hapke theory has a clear physical concept on photon transport in complex medium. The theory handles both isotropically and anisotropically

scattering of light interaction within the medium. It defines a volume-average extinction efficiency Q_E (unit: $m^2 \cdot m^{-2}$) — the ratio of light extinction cross-sectional area of particles to their geometrical cross-sectional area, for either uniform or non-uniform medium with either isotropic or anisotropic scatters. The light extinction (equivalent to interception) includes scattering (S) and absorption (A). The volume-average light extinction coefficient (E, $E=S+A$) is calculated as the total extinction efficiency for all particles in the medium. Base on extinction coefficient, the particle single-scattering albedo ω is defined as the ratio of scattering coefficient to extinction coefficient: $\omega = S/(S+A)$, and used in the radiative transfer equation. The solution to the equation was used hereto derive PPI.

For anisotropically scattering of light within canopy, a volume-average asymmetry factor β (linked to the phase function of scattering) is introduced in the scattering coefficient $S(1-\beta)$. Here $\beta = 0$ for isotropically scattering, and positive for predominantly forward-scattering (transmission) and negative for predominantly back-scattering (reflection) than the isotropic situation. Therefore the volume-average scattering albedo ω'

$$\omega' = \frac{S(1-\beta)}{S(1-\beta)+A} = \frac{1-\beta}{1-\omega\beta}\omega, \tag{16}$$

follows a similarity relation (Hapke, 1993) in radiative transfer equations.

For infinitely thick canopy, there is a relation between the diffusive reflectance r and albedo ω

$$\omega = \frac{4r}{(1+r)^2}. \tag{17}$$

Eq. (17) provides a simple method to estimate single leaf albedo from satellite measured reflectance above thick canopy. These leaf albedo estimates are useful for the operational FPAR modelling over large areas (Majasalmi et al., 2014; Stenberg et al., 2013).

3.3.2 PPI formulation and application

The diffusively reflected energy brings the interior information of a medium, such as optical depth or medium density, which can be estimated from the reflectance. In the case of vegetation, the optical depth is canopy LAI, and the involved light energy is the red and NIR. The red light is directly linked to vegetation photosynthesis, and the NIR is a spectrum for distinguishing green vegetation from others owing to its intercellular structure (Clark, 1946). However, in principle it is difficult to estimate canopy LAI from above canopy reflectance without knowing soil background reflectance (Verstraete et al., 1990). With some practical assumptions to deal with the unknown soil background influence, we used the difference between red and NIR reflectance in PPI to relate to LAI.

Many other issues are relieved by using nadir-viewing standardized reflectance in PPI calculation, such as sun-view geometry influences, and specular reflectance of leaf surface. The vegetation clumping is addressed by volume averaged property, so-called effective-medium theory of electromagnetic behavior in a geometrically complex medium (Hapke, 1993). The canopy and shoot clumping has great influences on radiation-based LAI measurements (Ryu et al., 2010; Chen, 1996; Stenberg, 1996), which is probably because such measurements are carried out within the medium (forest stand).

PPI uses a logarithm expression to attain a linear relationship with LAI. Such exponential or logarithm expression is common in reflectance spectroscopy. Using a logarithm transformation of vegetation index to relate to LAI has been tested in other studies (e.g. Gong et al., 1995), but there were few studies showing physical principles behind the logarithm expression.

The field test and modelling results confirmed the linearity of PPI to LAI. The snow influences on PPI signal is greatly suppressed. The noise shown in NDVI and EVI during snow season and the phenology transition periods is greatly reduced in PPI. Compared with other vegetation indices, the PPI time series better resembles plant growth process shown in GPP and manual phenology observations. These results suggest that PPI is useful for phenology retrieval, especially for overcoming the difficulties in remote sensing phenology over boreal forests.

We previously showed in Figure 11a the comparison between PPI and NDVI temporal profiles derived from MODIS NBAR data for the period 2000-2013 at the Abisko forest site. The PPI curve clearly shows influences of severe insect outbreaks in 2004 (Heliasz et al., 2011) and 2013 (H. Bylund, pers. comm). It also reveals that such severe insect attacks were preceded by 1-2 years of decreasing peak PPI values before a big outbreak, which gives some implications for forest pest control strategies. By contrast, the NDVI curve had slight changes during the years of severe insect outbreaks, but the preceding years of decreasing were not clear in the NDVI curve. This is mostly due to the fact that the understory vegetation made the NDVI signal close to a saturation level of the peak growth in ordinary years. In short, PPI had promising performances in characterizing disturbances of deciduous trees with suppressed understory effects on VI signals.

3.4 Phenology at European northern latitudes (Paper IV)

From the PPI derived phenology metrics, SOS, EOS, LOS and the PPI integral, we found that there were significant phenology trends and climate sensitivities in most parts of the study region for the period 2000-2014. On average SOS has advanced 0.39 days·year^{-1}, EOS has delayed 0.48 days·year^{-1}, LOS has extended 0.87

days·year^{-1}, and the PPI integral has increased 0.79%·year^{-1}. These trends have some spatial variations to different degrees. The trends for each country from Theil-Sen slope estimator are shown in Figure 13. These trends were estimated to be statically significant in panel data analysis, but the trend values reported by the Theil-Sen slope estimator are more robust against outliers. Figure 13 shows that in most countries SOS has advanced and consequently LOS has extended. The EOS had considerable variations; and it was close to zero in Norway, Sweden and Finland, and a large EOS delay was seen in the Netherlands, Germany and Poland. The prominent EOS delay resulted in much longer extension of growing season in the Netherlands, Germany and Poland than in the three Nordic countries.

Interestingly, the PPI integral, a proxy for vegetation production during the growing season also presents large spatial variations. The PPI integral did not generally change in Norway, Finland and Denmark, while other countries have seen increasing trends from 0.48 to 1.56 %·year^{-1}.

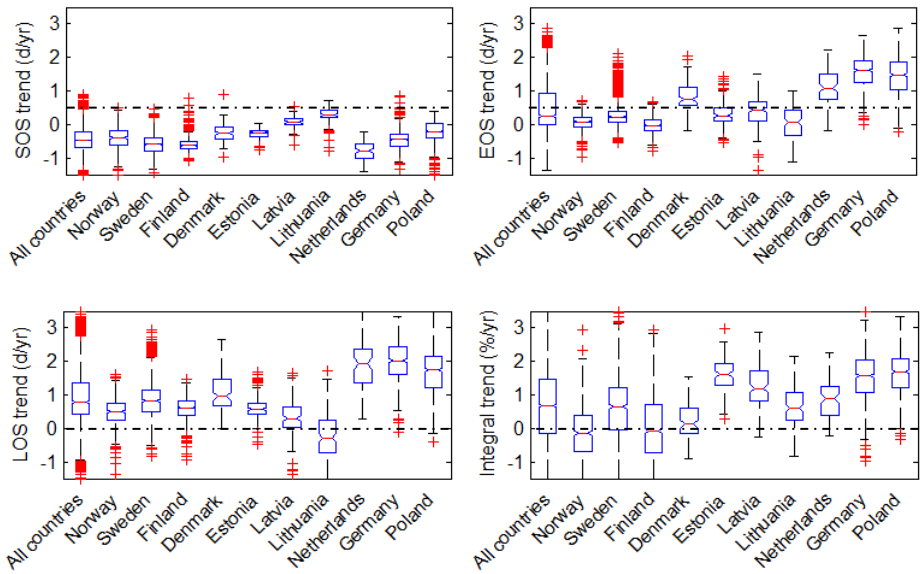

Figure 13. Phenology trends in each countries.

We further explored the phenology trends of different land cover types in the four Nordic countries (Figure 14). The most striking feature of these trends is that although the growing season has extended in these four countries in almost all land cover types owning to the advancement of SOS, the PPI integral did not increase correspondingly. In Norway, the LOS in urban area has hardly changed, but its PPI integral decreased at a rate of -1.19%·year^{-1}, along with the decreased PPI integral of other land cover types in the country. In Sweden, the evergreen needleleaf forests had an increasing rate of 0.72%·year^{-1} in the PPI integral,

whereas in Denmark the agriculture landcover had a decreasing trend of -0.16%·year^{-1} in the PPI integral. Taking the PPI integral as an indicator of plant production, these PPI integral trends may reflect the output variations in forestry and agricultural industries in these countries. These speculations need further studies to reach a convincing assessment.

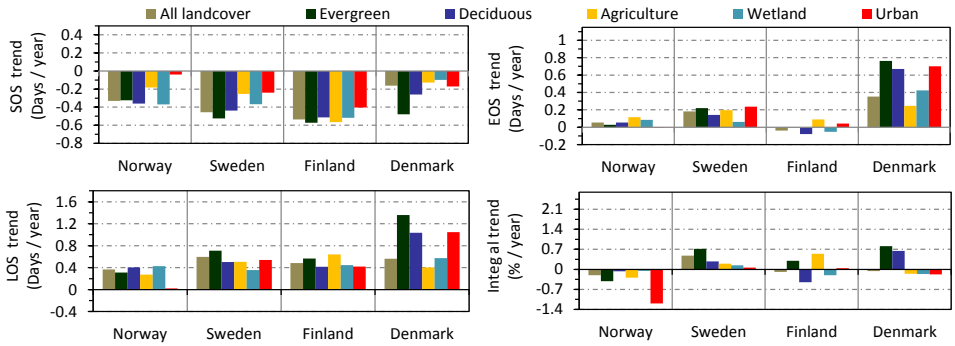

Figure 14. Phenology trends of different land covers in four Nordic countries

The estimated phenology trends were linked to phenology climate sensitivities. We found that in most parts of the study area, these phenology metrics have statistically significant relationship with temperature and precipitation for the period 2000-2014. The SOS advanced by 3.43 days·°C^{-1} and by 0.28 days·cm^{-1}; the EOS delayed by 1.27 days·°C^{-1} and by 0.05 days·cm^{-1}; the LOS extended by 3.16 days·°C^{-1} and shortened by 0.04 days·cm^{-1}; and the PPI integral increased by 2.29%·°C^{-1} and decreased by 0.07%·cm^{-1}. Precipitation had effects on phenology generally opposite to that of temperature, primarily over the three Nordic countries (Norway, Sweden, and Finland). Such precipitation sensitivities are probably due to the fact that more precipitation, regarding snowfall, was linked to cooler temperature, and regarding rainfall, was linked to less solar radiation reaching the land surface for photosynthesis. Among these general spatial sensitivity patterns, there were local variations. In the southern part of the study region (< 55ºN), more precipitation also led to delayed EOS, extended LOS and increased PPI integral, similar to the warming temperature effects on these phenology metrics.

These phenology metrics were found to have significant relationship with the North Atlantic Oscillation and Arctic Oscillation indices. These two atmospheric circulation patterns had similar influences on plant phenology and their correlation with SOS was stronger than with other phenology metrics.

4. Conclusions

In this thesis, a series of methods has been developed or employed to improve the phenology retrieval from satellite remote sensing data for a better understanding of the relationship between plant phenology and climate drivers at European northern latitudes. These methods include a proper design of ground spectral towers for calibration and validation of satellite measurements of vegetation, a reliable and easy *in situ* calibration method for long-term ground spectral sampling, a new algorithm for retrieving boreal forest phenology, and finally a non-parametric method and panel data analysis for estimating robust or statistically significant phenology trends and climate sensitivities. These methods will enable improved vegetation monitoring and phenology retrieval using remotely-sensed data from ground spectral towers or satellites. The results of phenology patterns, trends and climate sensitivities provide new insights into how plant phenology events spatially and temporally respond to climate variations at European northern latitudes in the new century, and demonstrate the potential of using PPI for improved phenology studies over large areas.

The main conclusions of the thesis can be summarized as:

- In the ellipse footprint of a ground spectral tower, the light sensor non-uniformly samples the target vegetation. The sampling points follow a Cauchy distribution that is centered at the tower. The sampling center shifts toward the sensor focus by considering the sensor directional response function.
- The regular *in situ* calibration of light sensors can be conducted easily and reliably by users. The results can be more accurate than manufacturer lab calibration if our procedures are followed.
- The plant phenology index (PPI) developed here shows great potential for retrieving phenology of boreal coniferous forests with enhanced representation of conifers growth activities and suppressed snow influences on satellite signals.
- Significant trends and climate sensitivities were estimated for most parts of the European northern latitudes (~90% of all valid grid cells). SOS has advanced and the growing season has extended at most parts for the years 2000-2014. Stronger positive trends in EOS and the PPI integral were observed in the southern part of the region than in the northern part. Temperature and precipitation have generally opposite effects on SOS,

LOS, and the PPI integral. The warming has overall led to advanced SOS, extended LOS, and increased PPI integral, whereas the wetting has led to delayed SOS, shortened LOS and decreasing PPI integral.

5. Outlook

5.1 PPI from other satellites or ground spectral towers

The MODIS-derived BRDF-corrected reflectance was used for generating PPI time series data. Such corrected reflectance can also be derived from other satellite or ground spectral tower measurements. The MODIS NBAR product employs a kernel-driven linear combination of three reflectances from a medium: isotropic, volumetric and geometric reflectance (Schaaf et al., 2002). Such an algorithm developed by Roujean et al. (1992), has also been used for deriving sun-view geometry corrected reflectance from AVHRR (Leroy and Roujean, 1994). With more than 30 years' of AVHRR data, we may use PPI to improve the estimation of global phenology variations during the past 3+ decades. It is also possible to derive PPI from Meteosat Second Generation at high temporal resolution or European Sentinel 2 at high spatial resolution for fine-resolution studies of plant phenology and growth processes.

Overall in this thesis, the connection is obvious between decadal atmospheric oscillations, climate variations, and plant phenology events. The climate-plant phenology connection may influence the consequent decadal events of animals that feed on plants, such as severe insect outbreaks. PPI computed from different data sources would improve the understanding of the interconnection between these events.

5.2 Estimation of global production from PPI

We showed good correlation between PPI and GPP, and that the PPI integral may be used to infer canopy production during growing season. An assessment of global GPP variations over past decades using PPI over large areas might be possible.

A recent study using VOD from the passive microwave remote sensing by Liu et al. (2015) estimated that globally there was a decreasing trend in the above-ground biomass carbon (ABC) from 1993 to 2012, which was mainly caused by the faster carbon loss in tropical forests than the net carbon gain by boreal and temperate forests and other vegetation.

We show the Liu et al. (2015)'s data for our study area in Figure 15. Among large areas of no trend estimation due to surface water issues in VOD, the overall decreasing trend of ABC in European temperate and boreal forests contradicts our results of overall increasing trends of the PPI integral (the figure on the front cover) and is counterintuitive to the extension of growing season in our study and many other studies. We previously showed that the VOD from AMSR-E (Advanced Microwave Scanning Radiometer - EOS) cannot reliably characterize the boreal forest growth at European northern latitudes due to long period of snow cover, soil water moisture, and coarse spatial resolution. Therefore with the PPI integral, a more reliable estimation of carbon sequestration over boreal forest may be achieved.

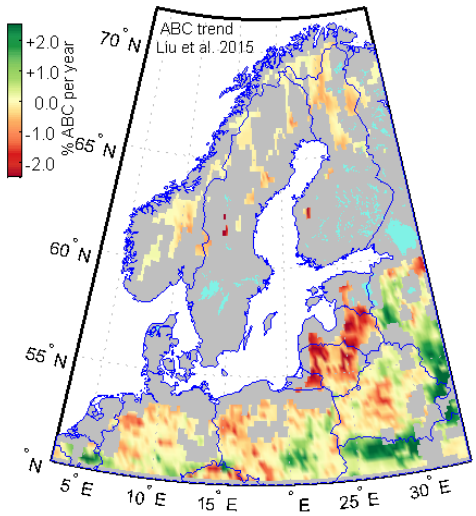

Figure 15. The trend of Aboveground Biomass Carbon (ABC) for the period 2000-2012. Data from passive microwave-based global aboveground biomass carbon dataset (1993-2012) version 1.0 (http://www.wenfo.org/wald/global-biomass/).

5.3 Phenology modelling

Satellite observed SOS can be used in plant phenology modelling. The current spring and autumn phenology models are mostly empirical and primarily based on temperature (Olsson and Jönsson, 2014). With PPI-derived phenology and gridded temperature data, pixel-wised thermal forcing can be estimated. An example is shown in Figure 16a for the SOS forcing requirement using the BC model, a day-length-adjusted forcing model (Olsson and Jönsson, 2014; Blümel and Chmielewski, 2012). From the estimated critical forcing requirements, the SOS of

other years can be modelled from temperature. An estimated SOS in 1950 is shown in Figure 16b. The usefulness of such a modelling exercise is manifold: 1) for studying phenology trends over past decades at regional or global scale; 2) for improving phenology models against ground observation; and 3) as input for Dynamic Global Vegetation Models (DGVM) to better represent seasonal vegetation growth. A recent study by Piao et al. (2015) argued that daily maximum temperature affects spring leafing stronger than daily mean temperature. PPI provides another possibility for testing this argument, from both PPI-derived phenology and PPI-based phenology modelling.

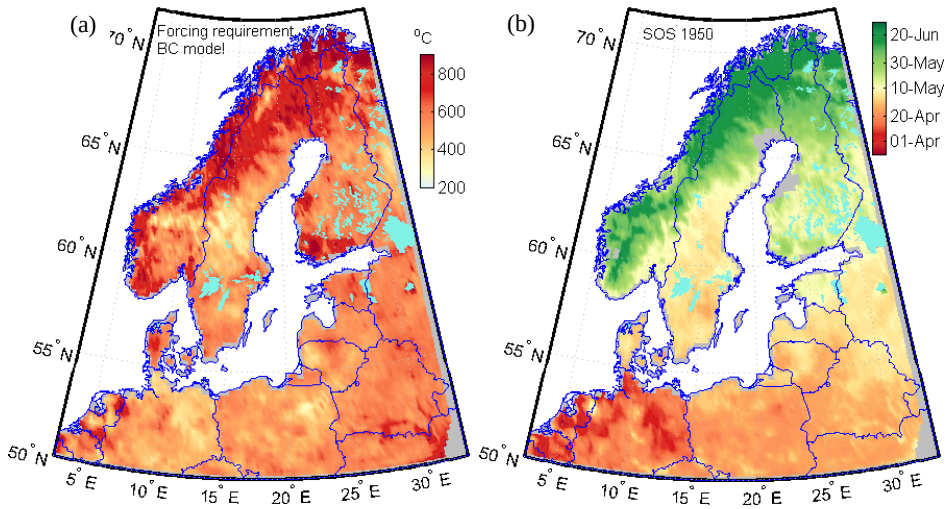

Figure 16. (a) Critical forcing requirement for the BC model, determined from PPI-derived phenology and gridded daily mean temperature. (b) Modelled SOS in 1950 from the forcing requirement and gridded temperature in 1950.

5.4 A PPI sensor

Base on the *in situ* calibration method in Paper II and the PPI algorithm in Paper III, it is possible to invent a PPI sensor for measuring LAI over crops or grass of low vegetation. The current most common methods for LAI measurement, the LAI-2000 Plant Canopy Analyzer and hemispherical photography, are primarily suitable for measuring forest canopy LAI. A PPI sensor is composed of a pair of hemispherical viewing sensors with NIR and red channels on each sensor. The calibration of such a sensor pair even does not need a white reference panel. The *in situ* calibration can be easily conducted by pointing them vertically toward the sky. Moreover, the parameters needed for calculating PPI, e.g. the soil reflectance and the maximum reflectance for dense vegetation can be measured.

Besides LAI measurements for scientific studies, another possible use of a PPI sensor is in the agriculture industry. By mounting such a sensor onto a tractor, PPI can be recorded with the tractor rolling over the field. The fertilizer and water spray could thus be regulated based on the crop growing condition that is translated from the PPI signal. A PPI sensor is expected to be more sensitive to crop stress than existing commercial NDVI sensors currently used in the agriculture industry.

Appendix

Appendix A1. Table of recent phenology studies

Table A1 Recent phenology studies with results about phenology trends (days·year^{-1})

Research	Time span	Location	Data	Type	SOS	EOS	LOS	Resolution or Note
Wang et al. (2015)	1982-2011	NH 30°-75°N	AVHRR/MODIS/SPOT	NDVI	**-0.14**			Resamp10 km
	1982-2011	N America	AVHRR/MODIS/SPOT	NDVI	-0.08			Resamp10 km
	1982-2011	Eurasia	AVHRR/MODIS/SPOT	NDVI	**-0.17**			Resamp10 km
	2000-2011	NH 30°-75°N	AVHRR GIMMS3g	NDVI	0.10			15 day 8 km
	2000-2011	NH 30°-75°N	MODIS MOD13A2	NDVI	-0.12			16 day 1km
	2000-2011	NH 30°-75°N	SPOT	NDVI	-0.53			10 day 1 km
Keenan et al. (2014)	2001-2012	E USA	MODIS MOD09GA	EVI/NDV/, GCC	**-0.48**	Different		Daily 500m
Jeganathan et al. (2014)	1982-2006	NH > 45°N-	GIMMS NDVI	NDVI	**-0.58**	**+0.64**		15 day 8 km
Fu et al. (2014)	1982-2011	W C Europe	AVHRR GIMMS 3g	NDVI	**-0.48**			15 day 8 km
	1982-1999	W C Europe	AVHRR GIMMS 3g	NDVI	**-1.24**			15 day 8 km
	2000-2011	W C Europe	AVHRR GIMMS 3g	NDVI	0.66			15 day 8 km
Zhang et al. (2014)	1982-2010	Europe	AVHRR GIMMS 3g	EVI2	No overall significant trends			15 day 8 km/daily
Karlsen et al. (2014)	2000-2013	Svalbard	MODIS MOD09Q1	NDVI	No overall significant trends			8 day 250m
Barichivich et al. (2013)	1982-2011	Eurasia	AVHRR GIMMS 3g	NDVI	**-0.18**	0.08	**0.25**	15 day 8 km
	1982-2011	N America	AVHRR GIMMS 3g	NDVI	0.01	**0.13**	0.10	15 day 8 km
Høgda et al. (2013)	1982-2011	Fennoscandia	AVHRR GIMMS 3g	NDVI	**-0.39**			15 day 8 km
	1982-1991	Fennoscandia	AVHRR GIMMS 3g	NDVI	**-1.46**			15 day 8 km
	1991-2001	Fennoscandia	AVHRR GIMMS 3g	NDVI	-0.48			15 day 8 km
	2001-2011	Fennoscandia	AVHRR GIMMS 3g	NDVI	-0.19			15 day 8 km

	2001-2011	Fen. N Oceanic	AVHRR GIMMS 3g	NDVI	**+0.49**			15 day 8 km
O'Connor et al. (2012)	2003-2009	Iceland	MERIS	MGVI	No overall significant trends			10day 1.2km
Jeong et al. (2011)	1982-2008	NH	AVHRR GIMMS g	NDVI	-0.13	**0.28**	0.39	15 day 8 km
	1982-1999	NH	AVHRR GIMMS g	NDVI	-0.28	**0.26**	0.56	15 day 8 km
	2000-2008	NH	AVHRR GIMMS g	NDVI	-0.02	0.29		15 day 8 km
	1982-2001	NH	AVHRR GIMMS g	NDVI	-0.35		0.65	15 day 8 km
	2000-2008	Europe	AVHRR GIMMS g	NDVI	-0.32	0.82		15 day 8 km
Zeng et al. (2011)	2000-2010	NH > 60°N	MODIS & AVHRR	NDVI	-0.47	0.16		Multi resolution
	2000-2010	N America	MODIS MOD13C1	NDVI	-1.15	0.22	**1.36**	16 day 0.05°
	1982-2008	N America	AVHRR GIMMSg	NDVI	-0.03	**0.27**	**0.29**	15 day 8 km
	2000-2010	Eurasia	MODIS MOD13C1	NDVI	-0.27	0.35	0.62	16 day 0.05°
	1982-2008	Eurasia	AVHRR GIMMS g	NDVI	-0.08	**0.64**	**0.72**	15 day 8 km
Julien and Sobrino (2009)	1981-2003	Global	AVHRR GIMMS g	NDVI	-0.38	0.45	0.80	15 day 8 km
	1981-2003	Europe	AVHRR GIMMS g	NDVI	-0.63	0.19	0.88	15 day 8 km
Karlsen et al. (2009)	1982-2006	Fennoscandia	AVHRR GIMMS g	NDVI	-0.27	**0.37**	**0.64**	15 day 8 km
White et al. (2009)	1982- 2006	N America	AVHRR GIMMS g	NDVI	No overall significant trends			15 day 8 km
Maignan et al. (2008)	1982-1999	Europe	AVHRR PAL	DVI	No trend analysis			10 day 8 km
Piao et al. (2006)	1982-1999	China	AVHRR GIMMS g	NDVI	-0.79	0.37	1.16	15 day 8 km
Reed (2006)	1982- 2003	N America	AVHRR GIMMS g	NDVI	No overall significant trends			15 day 8 km
de Beurs and Henebry (2005)	1985-1999	N America	AVHRR PAL	NDVI	-0.62			10 day 8 km
	1985-2000	Eurasia	AVHRR PAL	NDVI	-0.42			10 day 8 km
Stöckli and Vidale (2004)	1982-2001	Europe	AVHRR PAL	NDVI	**-0.54**	**0.42**	**0.96**	10 day 8 km
	1982-2001	Scandinavia	AVHRR PAL	NDVI	**-0.48**	**0.44**	**0.92**	10 day 8 km
	1982-2001	Germany	AVHRR PAL	NDVI	**-1.41**	**-0.04**	**1.38**	10 day 8 km
Zhou et al. (2001)	1981-1999	N America	AVHRR GIMMS g	NDVI	-0.43	0.23	**0.66**	15 day 8 km
	1981-1999	Eurasia	AVHRR GIMMS g	NDVI	**-0.36**	0.62	**0.97**	15 day 8 km
Tucker et al. (2001)	1982-1991	NH 45-75°N	AVHRR GIMMS g	NDVI	-0.56		0.39	15 day 8 km
	1992-1999	NH 45-75°N	AVHRR GIMMS g	NDVI	-0.21		0.05	15 day 8 km

Høgda et al. (2001)	1982-1998	Fennoscandia	AVHRR GIMMS g	NDVI	-0.82	0.62		15 day 8 km
Myneni et al. (1997)	1981-1991	Global	AVHRR PAL GIMMS	NDVI	-0.73		1.09	Multi resolution
Fu et al. (2014)	1982-2011	W C Europe	PEP725	Ground	-0.42			10^6+ data
	1982-1999	W C Europe	PEP725	Ground	-0.67			
	2000-2011	W C Europe	PEP725	Ground	-0.38			
Menzel et al. (2006)	1971-2000	Europe	COST725	Ground	-0.25	0.02		125000 data
Ahas et al. (2002)	1951-1998	Baltic region	POSITIVE	Ground	**-0.45**			Birch leafing
Chmielewski and Rötzer (2001)	1969-1998	Europe	IPG	Ground	-0.27	0.09	0.35	4 species in 67 sites
	1969-1998	Norway Ocean. Mt. area	IPG	Ground	-0.09	0.02	0.06	2 sites
Menzel (2000)	1959–1996	Europe	IPG	Ground	-0.21	0.15	0.36	751 spr. 281 aut. dat
Schwartz and Reiter (2000)	1959-1993	N USA	Lilac & SI first leaf	Ground/ TMP	**-0.18**			Lilac 1st lea date
Menzel and Fabian (1999)	1959–1993	Europe	IPG	Ground	-0.20	0.16	0.36	616 spring, 178 autumn data
Irannezhad and Kløve (2015)	1961–2011	Finland	FMI	Temp	**-0.16**		**0.30**	Daily 10 km
Barichivich et al. (2013)	1982-2011	NH > 45°N	HadGHCND	Temp			**0.35**	Daily 2.75°x3.75°
	1982-2011	Eurasia	HadGHCND	Temp	**-0.23**	**0.16**	**0.42**	Daily 2.75°x3.75°
	1982-2011	N America	HadGHCND	Temp	+0.02	**0.20**	0.21	Daily 2.75°x3.75°
Linderholm et al. (2008)	1951–2000	Greater Baltic	ECA&D	Temp	-0.13	0.02	0.15	36 daily TMP sites

Note:

1. **Bold** numbers are statistically significant trends ($p < 0.05$) specified in the corresponding studies, others without given significance level or with specified insignificance are due to short period, large inter-annual variation, or uncertainties in phenology retrieval.
2. Shaded rows are studies that have spatial overlap with this study.

Appendix A2. Mathematical derivations

In this section I provide detailed mathematic derivations of the main equations in the attached papers. This may enlighten other studies, and most important the readers can point out imperfections in the deductions, for further improvements.

A2.1 Cauchy distribution of ground sampling points

We use a Cartesian coordinate system (x,y,z) with the origin O at the center of the footprint ellipse (Figure A1). A sensor with an FOV of β and an off-nadir angle α, at a height H, is at (L,0,H), with its ground projection at (L,0,0).The sensor is viewing at a ground point (x,y,0) with a zenith angle θ, and an azimuth angel φ.

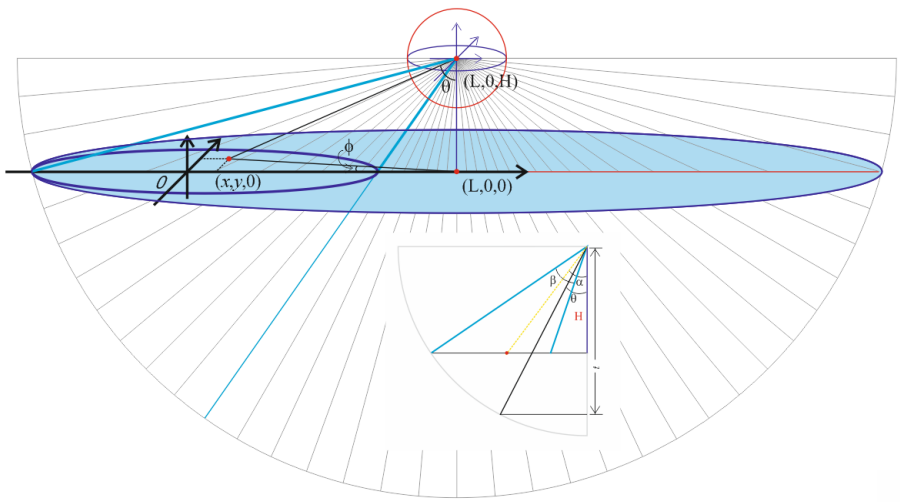

Figure A1. Derivation of the Cauchy distribution.

The relation between viewing geometry (θ,φ) and the ground point (x,y,0) is:

$$\begin{cases} \tan(\theta) = \sqrt{(x-L)^2 + y^2}\,/\,H \\ \tan(\varphi) = y/(x-L) \end{cases}, \tag{A1}$$

Where $L = \frac{H}{2}\left[\tan(\alpha + \frac{\beta}{2}) + \tan(\alpha - \frac{\beta}{2})\right]$

For a sensor with isotropic response, a viewing beam is uniformly distributed with in the cone. To realize a uniform sampling of the viewing beam, it needs to uniformly sample the sphere surface subtended by the sensor FOV.

Uniformly sampling a sphere surface is realized by:
$\varphi \in U(-\pi, \pi)$, and sampling the distribution of θ, which is via

$\cos(\theta) = \frac{t}{H / \cos(\alpha + \beta/2)}$, where $t \in U(H, H/\cos(\alpha+\beta/2))$.

Thus the θ has this distribution by using the inverse method:

$$f(\theta) = f(t(\theta))|t'(\theta)| = \frac{1}{H/\cos(\alpha+\beta/2) - H} H/\cos(\alpha+\beta/2)\sin(\theta)$$

$$= \frac{1}{1-\cos(\alpha+\beta/2)} \cdot \frac{\sqrt{(x-L)^2+y^2}}{\sqrt{(x-L)^2+y^2+H^2}}$$

From Eq. (A1) and Figure A1 it can be shown

$$\begin{cases} x = L - H\tan(\theta)\cos(\varphi) \\ y = H\tan(\theta)\sin(\varphi) \end{cases}.$$

Using the inverse method again, the joint distribution of ground sampling point (*x*,*y*) is

$f(x,y) = f(\theta(x,y), \varphi(x,y)) \cdot |J|$, where the Jacobian determinant

$$J = \begin{vmatrix} \partial\theta/\partial x & \partial\theta/\partial y \\ \partial\varphi/\partial x & \partial\varphi/\partial y \end{vmatrix}$$

Since θ and φ are independent from each other, their joint distribution is the product of their marginal distributions.

$$f(\theta,\varphi) = f(\theta)\cdot f(\varphi) = \frac{1}{2\pi} \cdot \frac{1}{1-\cos(\alpha+\beta/2)} \cdot \frac{\sqrt{(x-L)^2+y^2}}{\sqrt{(x-L)^2+y^2+H^2}}.$$

For the Jacobian determinant, we have

$\theta = \text{atan}(\sqrt{(x-L)^2+y^2}/H)$, thus

$$\frac{\partial\theta}{\partial x} = \frac{H(x-L)}{(x-L)^2+y^2+H^2} \cdot \frac{1}{\sqrt{(x-L)^2+y^2}},$$

$$\frac{\partial\theta}{\partial y} = \frac{Hy}{(x-L)^2+y^2+H^2} \cdot \frac{1}{\sqrt{(x-L)^2+y^2}},$$

and $\varphi = \text{atan}[y/(x-L)]$, thus $\frac{\partial\varphi}{\partial x} = \frac{-y}{(x-L)^2+y^2}$, $\frac{\partial\varphi}{\partial y} = \frac{x-L}{(x-L)^2+y^2}$.

So

$J = \partial\theta/\partial x \cdot \partial\varphi/\partial y - \partial\theta/\partial y \cdot \partial\varphi/\partial x$

$$= \frac{H(x-L)}{(x-L)^2+y^2+H^2} \cdot \frac{1}{\sqrt{(x-L)^2+y^2}} \cdot \frac{x-L}{(x-L)^2+y^2}$$
$$- \frac{Hy}{(x-L)^2+y^2+H^2} \cdot \frac{1}{\sqrt{(x-L)^2+y^2}} \cdot \frac{-y}{(x-L)^2+y^2}$$

$$= H \frac{1}{(x-L)^2+y^2+H^2} \cdot \frac{1}{\sqrt{(x-L)^2+y^2}} \cdot$$

Thus

$$f(x,y) = \frac{H}{2\pi} \cdot \frac{1}{1-\cos(\alpha+\beta/2)} \cdot \frac{1}{\left[(x-L)^2+y^2+H^2\right]^{3/2}}$$

is a Cauchy distribution.

A2.2 Tower influences

We denote *d*-tower width, *H*-tower height, *l*-boom length (Figure A2).

Tower shadow

The downward-looking sensor has a 180º FOV, and the shadow area is $d \times r$ ($r \leq R$). *r*- shadow length, *R*- the radius of hemispherical viewing area (πR^2). *R* is approximated by 10H (analyzed from sensor footprint model)

The fraction of shadow area:

$$f_S = \frac{d \cdot r}{\pi \cdot R^2} <= \frac{d}{\pi \cdot R} \approx \frac{d}{10\pi \cdot H} .$$

Blocked view

The blocked solid angle by the tower is

$$\Omega = \int_0^H \frac{d \cdot dh \cdot \cos\alpha}{l^2+h^2} = \int_0^H \frac{l}{\sqrt{l^2+h^2}} \frac{d \cdot dh}{l^2+h^2} = l \cdot d \cdot \int_0^H \frac{1}{(l^2+h^2)^{3/2}} dh$$

$$= l \cdot d \cdot \frac{h}{l^2 \cdot \sqrt{l^2+h^2}} \Big|_0^H = \frac{dH}{l\sqrt{H^2+l^2}}$$

$$\approx \frac{d}{l} \text{ for } l < 0.1H .$$

Thus the fraction of the sensor viewing solid angle blocked by the tower (the ratio of the blocked solid angle to the whole projected solid angle π of downward-looking sensor):

$$f_\Omega \approx \frac{d}{\pi l} .$$

Using the viewing proportion being blocked by a spectral tower, and the tower surface reflectance, the tower influences on the measured reflectance signal can be estimated.

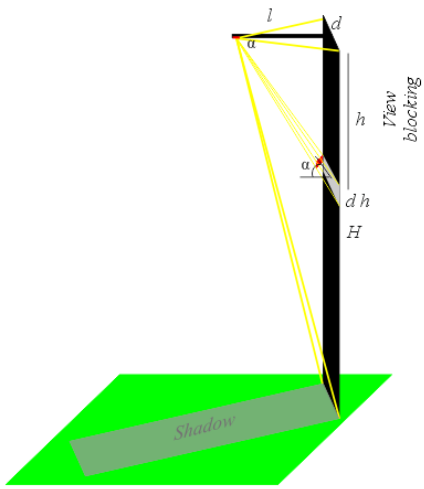

Figure A2. Derivation of tower influcences.

A2.3 Uncertainty propagation

Here we provide the standard uncertainty in a normalized difference vegetation index, such as NDVI and PRI, NDWI (Gao, 1996), and etc. that is propagated from reflectance uncertainty due to calibration. We take NDVI as an example in the derivation.

From $NDVI = \frac{NIR - red}{NIR + red}$, we get

$$\frac{\partial \ln(NDVI)}{\partial NIR} = \frac{1}{NDVI} \cdot \left(\frac{1}{NIR + red} - \frac{NIR - red}{(NIR + red)^2}\right)$$

$$= \frac{1}{NDVI} \cdot \frac{2red}{(NIR + red)^2}$$

Similarly $\frac{\partial \ln(NDVI)}{\partial red} = \frac{1}{NDVI} \cdot \frac{-2NIR}{(NIR + red)^2}$

Relative standard uncertainty propagation is

$$\frac{u(NDVI)}{NDVI} = \sqrt{\left(\frac{\partial \ln(NDVI)}{\partial red} u(red)\right)^2 + \left(\frac{\partial \ln(NDVI)}{\partial NIR} u(NIR)\right)^2}$$

$$= \sqrt{\left(\frac{1}{NDVI} \cdot \frac{-2NIR}{(NIR+red)^2} u(red)\right)^2 + \left(\frac{1}{NDVI} \cdot \frac{2red}{(NIR+red)^2} u(NIR)\right)^2}$$

$$= \frac{1-NDVI^2}{2NDVI} \cdot \sqrt{\left(\frac{u(red)}{red}\right)^2 + \left(\frac{u(NIR)}{NIR}\right)^2} \ .$$

Acknowledgements

I express my most sincere thanks to my main supervisor Prof. Lars Eklundh in remote sensing and GIS who shows great foresight from a high plane. My PhD study under his umbrella is probably the only chance in my career of doing a free-style research from field to lab, from space to ground, from experiment to modelling, and from theory to application. I feel I take no risk in what I am doing because he is always there, together with a strong co-supervisory team, which I had privileges to ask for helps anytime when I am lost in research. They are associate Prof. Anna Maria Jönsson in plant ecology, Prof. Per Jönsson in applied mathematics, and Dr. Johan Lindström in statistics.

Thanks to my INES colleagues. Your willingness to help and the friendly research environment always made me relaxed here like a holiday. Thanks to my fellow PhD students and those Chinese friends in the department. I really enjoyed the PhD activities and ping pong game with you. Thanks to my office-mate Cecilia Olsson. I always mistook you for a traditional Chinese lady with many of such similar virtues. I was lucky to share the same office, same PhD project, co-author my 4th thesis paper with you. Thanks for many discussions from research to personal life with you.

Thanks to Lars Eklundh, Cecilia Olsson, Ning Zhang, and Kangying Jin for proof reading the Kappa and valuable suggestions for improving it.

Lastly I give my thanks to my family, my wife Dr. Xianli Zhu and three kids Kanying Jin, Linda Jin and Luka Jin. Thanks for your patience with me struggling the tough life every day.

我既感激又愧对我的父母。他们年逾花甲，依然在老家侍弄十几亩薄田，鸡鸭牛羊为伴。父母满脸镌刻着岁月沧桑，满眼流露着对儿的殷切期盼。当乙未年春节这天收到妻兄传来老父母的照片，不由得使我泪流满面。年过不惑，浪迹他乡我为哪般。谨此拙作，以致父母。

To my parents, typical Chinese farmers

References

Abbe, C. (1905). *A first report on the relations between climates and crops*. Washington: Government Printing Office

Ahas, R., Aasa, A., Menzel, A., Fedotova, V.G., & Scheifinger, H. (2002). Changes in European spring phenology. *International Journal of Climatology, 22*, 1727-1738

Allen, W.A., & Richardson, A.J. (1968). Interaction of Light with a Plant Canopy. *J. Opt. Soc. Am., 58*, 1023-1028

Balzarolo, M., Anderson, K., Nichol, C., Rossini, M., Vescovo, L., Arriga, N., Wohlfahrt, G., Calvet, J.-C., Carrara, A., Cerasoli, S., Cogliati, S., Daumard, F., Eklundh, L., Elbers, J.A., Evrendilek, F., Handcock, R.N., Kaduk, J., Klumpp, K., Longdoz, B., Matteucci, G., Meroni, M., Montagnani, L., Ourcival, J.-M., Sánchez-Cañete, E.P., Pontailler, J.-Y., Juszczak, R., Scholes, B., & Martín, M.P. (2011). Ground-based optical measurements at European flux sites: a review of methods, instruments and current controversies. *Sensors, 11*, 7954-7981

Baret, F., Morissette, J.T., Fernandes, R.A., Champeaux, J.L., Myneni, R.B., Chen, J., Plummer, S., Weiss, M., Bacour, C., Garrigues, S., & Nickeson, J.E. (2006). Evaluation of the representativeness of networks of sites for the global validation and intercomparison of land biophysical products: proposition of the CEOS-BELMANIP. *IEEE Transactions on Geoscience and Remote Sensing, 44*, 1794-1803

Barichivich, J., Briffa, K.R., Myneni, R.B., Osborn, T.J., Melvin, T.M., Ciais, P., Piao, S., & Tucker, C. (2013). Large-scale variations in the vegetation growing season and annual cycle of atmospheric CO2 at high northern latitudes from 1950 to 2011. *Global Change Biology, 19*, 3167-3183

Blümel, K., & Chmielewski, F.-M. (2012). Shortcomings of classical phenological forcing models and a way to overcome them. *Agricultural and Forest Meteorology, 164*, 10-19

Campbell, G.S., & Norman, J.M. (1998). *An Introduction to Environmental Biophysics*: Springer-Verlag New York, Inc.

Campbell Scientific (2011). *CNR1 Net Radiometer Instruction Manual*. Logan, Utah, USA: Campbell Scientific, Inc. (CSI)

Chapman, B., Jost, G., & Pas, R.v.d. (2008). *Using OpenMP, Portable Shared Memory Parallel Programming*: Massachusetts Institute of Technology

Chen, J.M. (1996). Optically-based methods for measuring seasonal variation of leaf area index in boreal conifer stands. *Agricultural and Forest Meteorology, 80*, 135-163

Chmielewski, F.-M., & Rötzer, T. (2001). Response of tree phenology to climate change across Europe. *Agricultural and Forest Meteorology, 108*, 101-112

Clark, W. (1946). Infrared photography applied to botany and palaeontology. *Photography by infrared, its principles and applications* (pp. 253-274). New York: John Wiley & Sons

de Beurs, K.M., & Henebry, G.M. (2005). A statistical framework for the analysis of long image time series. *International Journal of Remote Sensing, 26*, 1551-1573

Delbart, N., Kergoat, L., Le Toan, T., Lhermitte, J., & Picard, G. (2005). Determination of phenological dates in boreal regions using normalized difference water index. *Remote Sensing of Environment, 97*, 26-38

Edström, P. (2010). *Simulation and modeling of light scattering in paper and print applications*: Springer-Verlag Berlin Heidelberg

EEA (2007). CLC2006 technical guidelines. In, *EEA Technical report No 17/2007*. Luxembourg: European Environment Agency

Eklundh, L., Jin, H., Schubert, P., Guzinski, R., & Heliasz, M. (2011). An optical sensor network for vegetation phenology monitoring and satellite data calibration. *Sensors, 11*, 7678-7709

Fensholt, R., Sandholt, I., & Rasmussen, M.S. (2004). Evaluation of MODIS LAI, fAPAR and the relation between fAPAR and NDVI in a semi-arid environment using in situ measurements. *Remote Sensing of Environment, 91*, 490-507

Fu, Y.H., Piao, S., Op de Beeck, M., Cong, N., Zhao, H., Zhang, Y., Menzel, A., & Janssens, I.A. (2014). Recent spring phenology shifts in western Central Europe based on multiscale observations. *Global Ecology and Biogeography, 23*, 1255-1263

Gamon, J.A., Serrano, L., & Surfus, J.S. (1997). The photochemical reflectance index: an optical indicator of photosynthetic radiation use efficiency across species, functional types, and nutrient levels. *Oecologia, 112*, 492-501

Gao, B. (1996). NDWI—A normalized difference water index for remote sensing of vegetation liquid water from space. *Remote Sensing of Environment, 58*, 257-266

Garrigues, S., Lacaze, R., Baret, F., Morisette, J.T., Weiss, M., Nickeson, J.E., Fernandes, R., Plummer, S., Shabanov, N.V., Myneni, R.B., Knyazikhin, Y., & Yang, W. (2008). Validation and intercomparison of global Leaf Area Index products derived from remote sensing data. *Journal of Geophysical Research: Biogeosciences, 113*, G02028

Gong, P., Pu, R., & Miller, J.R. (1995). *Coniferous forest leaf area index estimation along the Oregon transect using compact airborne spectrographic imager data*. Bethesda, MD, ETATS-UNIS: American Society for Photogrammetry and Remote Sensing

Hapke, B. (1993). *Theory of Reflectance and Emittance Spectroscopy*: Cambridge University Press

Harris, A., Gamon, J.A., Pastorello, G.Z., & Wong, C.Y.S. (2014). Retrieval of the photochemical reflectance index for assessing xanthophyll cycle activity: a comparison of near-surface optical sensors. *Biogeosciences, 11*, 6277-6292

Haylock, M.R., Hofstra, N., Klein Tank, A.M.G., Klok, E.J., Jones, P.D., & New, M. (2008). A European daily high-resolution gridded data set of surface temperature and precipitation for 1950–2006. *Journal of Geophysical Research: Atmospheres, 113*, D20119

Heliasz, M., Johansson, T., Lindroth, A., Mölder, M., Mastepanov, M., Friborg, T., Callaghan, T.V., & Christensen, T.R. (2011). Quantification of C uptake in subarctic birch forest after setback by an extreme insect outbreak. *Geophys. Res. Lett., 38*, L01704

Høgda, K., Tømmervik, H., & Karlsen, S. (2013). Trends in the Start of the Growing Season in Fennoscandia 1982–2011. *Remote Sensing, 5*, 4304-4318

Høgda, K.A., Karlsen, S.R., & Solheim, I. (2001). Climatic change impact on growing season in Fennoscandia studied by a time series of NOAA AVHRR NDVI data. In, *Geoscience and Remote Sensing Symposium, 2001. IGARSS '01. IEEE 2001 International* (pp. 1338-1340 vol.1333)

Holben, B.N. (1986). Characteristics of maximum-value composite images from temporal AVHRR data. *International Journal of Remote Sensing, 7*, 1417-1434

Hsiao, C. (2003). *Analysis of panel data*: Cambridge University Press

Huete, A., Didan, K., Miura, T., Rodriguez, E.P., Gao, X., & Ferreira, L.G. (2002). Overview of the radiometric and biophysical performance of the MODIS vegetation indices. *Remote Sensing of Environment, 83*, 195-213

IPCC (2014). *Climate Change 2014: Impacts, Adaptation, and Vulnerability. Part A: Global and Sectoral Aspects. Contribution of Working Group II to the Fifth Assessment Report of the Intergovernmental Panel on Climate Change*. Cambridge University Press, Cambridge, United Kingdom and New York, NY, USA

Irannezhad, M., & Kløve, B. (2015). Do atmospheric teleconnection patterns explain variations and trends in thermal growing season parameters in Finland? *International Journal of Climatology*, n/a-n/a

Jamali, S., Jönsson, P., Eklundh, L., Ardö, J., & Seaquist, J. (2015). Detecting changes in vegetation trends using time series segmentation. *Remote Sensing of Environment, 156*, 182-195

Jeganathan, C., Dash, J., & Atkinson, P.M. (2014). Remotely sensed trends in the phenology of northern high latitude terrestrial vegetation, controlling for land cover change and vegetation type. *Remote Sensing of Environment, 143*, 154-170

Jeong, S.-J., Ho, C.-H., Gim, H.-J., & Brown, M.E. (2011). Phenology shifts at start vs. end of growing season in temperate vegetation over the Northern Hemisphere for the period 1982–2008. *Global Change Biology, 17*, 2385-2399

Jones, L.A., & Kimball, J.S. (2011). Daily Global Land Surface Parameters Derived from AMSR-E. Boulder Colorado USA: National Snow and Ice Data Center. Digital media In

Jones, M.O., Jones, L.A., Kimball, J.S., & McDonald, K.C. (2011). Satellite passive microwave remote sensing for monitoring global land surface phenology. *Remote Sensing of Environment, 115*, 1102-1114

Jönsson, A.M., Eklundh, L., Hellström, M., Bärring, L., & Jönsson, P. (2010). Annual changes in MODIS vegetation indices of Swedish coniferous forests in relation to snow dynamics and tree phenology. *Remote Sensing of Environment, 114*, 2719-2730

Jönsson, A.M., Pulatov, B., Linderson, M.-L., & Hall, K. (2013). Modelling as a tool for analysing the temperature-dependent future of the Colorado potato beetle in Europe. *Global Change Biology*, n/a-n/a

Jönsson, P., & Eklundh, L. (2002). Seasonality extraction by function fitting to time-series of satellite sensor data. *Geoscience and Remote Sensing, IEEE Transactions on, 40*, 1824-1832

Jönsson, P., & Eklundh, L. (2004). TIMESAT—a program for analyzing time-series of satellite sensor data. *Computers & Geosciences, 30*, 833-845

Julien, Y., & Sobrino, J.A. (2009). Global land surface phenology trends from GIMMS database. *International Journal of Remote Sensing, 30*, 3495-3513

Karlsen, S., Elvebakk, A., Høgda, K., & Grydeland, T. (2014). Spatial and Temporal Variability in the Onset of the Growing Season on Svalbard, Arctic Norway — Measured by MODIS-NDVI Satellite Data. *Remote Sensing, 6*, 8088-8106

Karlsen, S., Ramfjord, H., Høgda, K., Johansen, B., Danks, F., & Brobakk, T. (2009a). A satellite-based map of onset of birch (Betula) flowering in Norway. *Aerobiologia, 25*, 15-25

Karlsen, S., Solheim, I., Beck, P., Høgda, K., Wielgolaski, F., & Tømmervik, H. (2007). Variability of the start of the growing season in Fennoscandia, 1982–2002. *International Journal of Biometeorology, 51*, 513-524

Karlsen, S.R., Høgda, K.A., Wielgolaski, F.E., Tolvanen, A., Tømmervik, H., Poikolainen, J., & Kubin, E. (2009b). Growing-season trends in Fennoscandia 1982-2006, determined from satellite and phenology data. *Climate Research, 39*, 275-286

Kasten, F., & Young, A.T. (1989). Revised optical air mass tables and approximation formula. *Applied Optics, 28*, 4735-4738

Keeling, C.D., Chin, J.F.S., & Whorf, T.P. (1996). Increased activity of northern vegetation inferred from atmospheric CO2 measurements. *Nature, 382*, 146-149

Keenan, T.F., Gray, J., Friedl, M.A., Toomey, M., Bohrer, G., Hollinger, D.Y., Munger, J.W., O/'Keefe, J., Schmid, H.P., Wing, I.S., Yang, B., & Richardson, A.D. (2014). Net carbon uptake has increased through warming-induced changes in temperate forest phenology. *Nature Clim. Change, 4*, 598-604

Keenan, T.F., & Richardson, A.D. (2015). The timing of autumn senescence is affected by the time of spring phenology: implications for predictive models. *Global Change Biology*, n/a-n/a

Knyazikhin, Y., Schull, M.A., Stenberg, P., Mõttus, M., Rautiainen, M., Yang, Y., Marshak, A., Latorre Carmona, P., Kaufmann, R.K., Lewis, P., Disney, M.I., Vanderbilt, V., Davis, A.B., Baret, F., Jacquemoud, S., Lyapustin, A., & Myneni, R.B. (2013). Hyperspectral remote sensing of foliar nitrogen content. *Proceedings of the National Academy of Sciences, 110*, E185–E192

Kubelka, P., & Munk, F. (1931). Ein Beitrag zur Optik der Farbanstriche. *Zeitschrift für technische Physik, 12*, 593–601

Kuusk, A. (1995). A Fast, Invertible Canopy Reflectance Model. *Remote Sensing of Environment, 51*, 342-350

Leroy, M., & Roujean, J.L. (1994). Sun and view angle corrections on reflectances derived from NOAA/AVHRR data. *Geoscience and Remote Sensing, IEEE Transactions on, 32*, 684-697

LI-COR (2009). *LAI-2200 Plant Canopy Analyzer: Instruction Manual*

Lieth, H. (1974). *Phenology and Seasonality Modeling (Ecological Studies-Analysis and Synthesis Series, Vol 8)*: Springer-Verlag

Linderholm, H.W., Walther, A., & Chen, D. (2008). Twentieth-century trends in the thermal growing season in the Greater Baltic Area. *Climatic Change, 87*, 405-419

Liu, Y.Y., van Dijk, A.I.J.M., de Jeu, R.A.M., Canadell, J.G., McCabe, M.F., Evans, J.P., & Wang, G. (2015). Recent reversal in loss of global terrestrial biomass. *Nature Clim. Change, advance online publication*

Maignan, F., Bréon, F.M., Bacour, C., Demarty, J., & Poirson, A. (2008). Interannual vegetation phenology estimates from global AVHRR measurements: Comparison with in situ data and applications. *Remote Sensing of Environment, 112*, 496-505

Majasalmi, T., Rautiainen, M., & Stenberg, P. (2014). Modeled and measured fPAR in a boreal forest: Validation and application of a new model. *Agricultural and Forest Meteorology, 189–190*, 118-124

Majasalmi, T., Rautiainen, M., Stenberg, P., & Manninen, T. (2015). Validation of MODIS and GEOV1 fPAR Products in a Boreal Forest Site in Finland. *Remote Sensing, 7*, 1359-1379

Mann, H.B., & Whitney, D.R. (1947). On a Test of Whether one of Two Random Variables is Stochastically Larger than the Other. *Ann. Math. Statist., 18*, 50-60

Menzel, A. (2000). Trends in phenological phases in Europe between 1951 and 1996. *International Journal of Biometeorology, 44*, 76-81

Menzel, A., & Fabian, P. (1999). Growing season extended in Europe. *Nature, 397*, 659-659

Menzel, A., Sparks, T.H., Estrella, N., Koch, E., Aasa, A., Ahas, R., Alm-KÜBler, K., Bissolli, P., BraslavskÁ, O.G., Briede, A., Chmielewski, F.M., Crepinsek, Z., Curnel, Y., Dahl, Å., Defila, C., Donnelly, A., Filella, Y., Jatczak, K., MÅGe, F., Mestre, A., Nordli, Ø., PeÑUelas, J., Pirinen, P., RemiŠOvÁ, V.,

Scheifinger, H., Striz, M., Susnik, A., Van Vliet, A.J.H., Wielgolaski, F.-E., Zach, S., & Zust, A.N.A. (2006). European phenological response to climate change matches the warming pattern. *Global Change Biology, 12*, 1969-1976

Morisette, J.T., Baret, F., Privette, J.L., Myneni, R.B., Nickeson, J.E., Garrigues, S., Shabanov, N.V., Weiss, M., Fernandes, R.A., Leblanc, S.G., Kalacska, M., Sanchez-Azofeifa, G.A., Chubey, M., Rivard, B., Stenberg, P., Rautiainen, M., Voipio, P., Manninen, T., Pilant, A.N., Lewis, T.E., Iiames, J.S., Colombo, R., Meroni, M., Busetto, L., Cohen, W.B., Turner, D.P., Warner, E.D., Petersen, G.W., Seufert, G., & Cook, R. (2006). Validation of global moderate-resolution LAI products: a framework proposed within the CEOS land product validation subgroup. *Geoscience and Remote Sensing, IEEE Transactions on, 44*, 1804-1817

Myneni, R.B., Keeling, C.D., Tucker, C.J., Asrar, G., & Nemani, R.R. (1997). Increased plant growth in the northern high latitudes from 1981 to 1991. *Nature, 386*, 698-702

O'Connor, B., Dwyer, E., Cawkwell, F., & Eklundh, L. (2012). Spatio-temporal patterns in vegetation start of season across the island of Ireland using the MERIS Global Vegetation Index. *Isprs Journal of Photogrammetry and Remote Sensing, 68*, 79-94

Olofsson, P., & Eklundh, L. (2007). Estimation of absorbed PAR across Scandinavia from satellite measurements. Part II: Modeling and evaluating the fractional absorption. *Remote Sensing of Environment, 110*, 240-251

Olsson, C., & Jönsson, A.M. (2014). Process-based models not always better than empirical models for simulating budburst of Norway spruce and birch in Europe. *Global Change Biology*, n/a-n/a

ORNL DAAC (2013). FLUXNET Web Page. In: Oak Ridge National Laboratory Distributed Active Archive Center

Pan, Y., Birdsey, R.A., Fang, J., Houghton, R., Kauppi, P.E., Kurz, W.A., Phillips, O.L., Shvidenko, A., Lewis, S.L., Canadell, J.G., Ciais, P., Jackson, R.B., Pacala, S.W., McGuire, A.D., Piao, S., Rautiainen, A., Sitch, S., & Hayes, D. (2011). A Large and Persistent Carbon Sink in the World's Forests. *Science, 333*, 988-993

Parmesan, C. (2007). Influences of species, latitudes and methodologies on estimates of phenological response to global warming. *Global Change Biology, 13*, 1860-1872

Parmesan, C., & Yohe, G. (2003). A globally coherent fingerprint of climate change impacts across natural systems. *Nature, 421*, 37-42

Pau, S., Wolkovich, E.M., Cook, B.I., Davies, T.J., Kraft, N.J.B., Bolmgren, K., Betancourt, J.L., & Cleland, E.E. (2011). Predicting phenology by integrating ecology, evolution and climate science. *Global Change Biology, 17*, 3633-3643

Piao, S., Fang, J., Zhou, L., Ciais, P., & Zhu, B. (2006). Variations in satellite-derived phenology in China's temperate vegetation. *Global Change Biology, 12*, 672-685

Piao, S., Tan, J., Chen, A., Fu, Y.H., Ciais, P., Liu, Q., Janssens, I.A., Vicca, S., Zeng, Z., Jeong, S.-J., Li, Y., Myneni, R.B., Peng, S., Shen, M., & Penuelas, J. (2015). Leaf onset in the northern hemisphere triggered by daytime temperature. *Nat Commun, 6*

Ratanamahatana, C., & Keogh, E. (2004). Making Time-Series Classification More Accurate Using Learned Constraints. In M.W. Berry (Ed.), *Proceedings of the Fourth SIAM International Conference on Data Mining* (pp. 11-22)

Reed, B.C. (2006). Trend Analysis of Time-Series Phenology of North America Derived from Satellite Data. *GIScience & Remote Sensing, 43*, 24-38

Reed, B.C., Brown, J.F., VanderZee, D., Loveland, T.R., Merchant, J.W., & Ohlen, D.O. (1994). Measuring phenological variability from satellite imagery. *Journal of Vegetation Science, 5*, 703-714

Richardson, A.D., Hollinger, D.Y., Dail, D.B., Lee, J.T., Munger, J.W., & O'Keefe, J. (2009). Influence of spring phenology on seasonal and annual carbon balance in two contrasting New England forests. *Tree Physiology, 29*, 321-331

Ross, J. (1981). *The Radiation Regime and Architecture of Plant Stands*: Springer

Roujean, J.-L., Leroy, M., & Deschamps, P.-Y. (1992). A bidirectional reflectance model of the Earth's surface for the correction of remote sensing data. *Journal of Geophysical Research: Atmospheres, 97*, 20455-20468

Rouse, J.W., Jr., R.H.H., Deering, D.W., & Schell, J.A. (1973). Monitoring the vernal advancement and retrogradation (green wave effect) of natural vegetation. In N.G.T.I.F. Report (Ed.) (p. 87). Goddard Space Flight Center, Greenbelt, Maryland, 20771

Ryu, Y., Sonnentag, O., Nilson, T., Vargas, R., Kobayashi, H., Wenk, R., & Baldocchi, D.D. (2010). How to quantify tree leaf area index in an open savanna ecosystem: A multi-instrument and multi-model approach. *Agricultural and Forest Meteorology, 150*, 63-76

Schaaf, C.B., Gao, F., Strahler, A.H., Lucht, W., Li, X., Tsang, T., Strugnell, N.C., Zhang, X., Jin, Y., Muller, J.P., Lewis, P., Barnsley, M., Hobson, P., Disney, M., Roberts, G., Dunderdale, M., Doll, C., d'Entremont, R.P., Hu, B., Liang, S., Privette, J.L., & Roy, D. (2002). First operational BRDF, albedo nadir reflectance products from MODIS. *Remote Sensing of Environment, 83*, 135-148

Schubert, P., Lagergren, F., Aurela, M., Christensen, T., Grelle, A., Heliasz, M., Klemedtsson, L., Lindroth, d., Pilegaard, K., Vesala, T., & Eklundh, L. (2012). Modeling GPP in the Nordic forest landscape with MODIS time series data — Comparison with the MODIS GPP product. *Remote Sensing of Environment, 126*, 136-147

Schwartz, M.D., & Reiter, B.E. (2000). Changes in North American spring. *International Journal of Climatology, 20*, 929-932

Sen, P.K. (1968). Estimates of the regression coefficient based on Kendall's tau. *Journal of the American Statistical Association, 63*, 1379-1389

Sjöström, M., Ardö, J., Eklundh, L., El-Tahir, B.A., El-Khidir, H.A.M., Hellström, M., Pilesjö, P., & Seaquist, J. (2009). Evaluation of satellite based indices for

gross primary production estimates in a sparse savanna in the Sudan. *Biogeosciences, 6*, 129-138
Sjöström, M., Zhao, M., Archibald, S., Arneth, A., Cappelaere, B., Falk, U., de Grandcourt, A., Hanan, N., Kergoat, L., Kutsch, W., Merbold, L., Mougin, E., Nickless, A., Nouvellon, Y., Scholes, R.J., Veenendaal, E.M., & Ardö, J. (2013). Evaluation of MODIS gross primary productivity for Africa using eddy covariance data. *Remote Sensing of Environment, 131*, 275-286
Skogs Industrierna (2013). The Swedish forest industries – Facts and Figures 2013. In (p. 60): Swedish Forest Industries Federation
Steinberg, D.C., Goetz, S.J., & Hyer, E.J. (2006). Validation of MODIS F/sub PAR/ products in boreal forests of Alaska. *Geoscience and Remote Sensing, IEEE Transactions on, 44*, 1818-1828
Stenberg, P. (1996). Correcting LAI-2000 estimates for the clumping of needles in shoots of conifers. *Agricultural and Forest Meteorology, 79*, 1-8
Stenberg, P. (2006). A note on the G-function for needle leaf canopies. *Agricultural and Forest Meteorology, 136*, 76-79
Stenberg, P., Lukeš, P., Rautiainen, M., & Manninen, T. (2013). A new approach for simulating forest albedo based on spectral invariants. *Remote Sensing of Environment, 137*, 12-16
Stöckli, R., & Vidale, P.L. (2004). European plant phenology and climate as seen in a 20 year AVHRR land-surface parameter dataset. *International Journal of Remote Sensing, 25*, 3303-3330
Strahler, A.H., Lucht, W., Schaaf, C.B., Tsang, T., Gao, F., Li, X., Muller, J.-P., Lewis, P., & Barnsley, M.J. (1999). MODIS BRDF/Albedo Product: Algorithm Theoretical Basis Document, Version5.0. In
Suehrcke, H., & McCormick, P.G. (1988). The diffuse fraction of instantaneous solar radiation. *Solar Energy, 40*, 423-430
Theil, H. (1950). A rank-invariant method of linear and polynomial regression analysis. *Proceedings of the Royal Netherlands Academy of Sciences, 53*, 386-392
Tømmervik, H., Johansen, B., Riseth, J., Karlsen, S.R., Solberg, B., Høgda, K.A., & Høgda, K.A. (2009). Above ground biomass changes in the mountain birch forests and mountain heaths of Finnmarksvidda, northern Norway, in the period 1957–2006. *Forest Ecology and Management, 257*, 244-257
Tucker, C.J. (1979). Red and photographic infrared linear combinations for monitoring vegetation. *Remote Sensing of Environment, 8*, 127-150
Tucker, C.J., Slayback, D.A., Pinzon, J.E., Los, S.O., Myneni, R.B., & Taylor, M.G. (2001). Higher northern latitude normalized difference vegetation index and growing season trends from 1982 to 1999. *International Journal of Biometeorology, 45*, 184-190
Verstraete, M.M., Pinty, B., & Dickinson, R.E. (1990). A physical model of the bidirectional reflectance of vegetation canopies. I. Theory. *Journal of Geophysical Research, 95*, 11,755-711,765
Visser, M.E., & Both, C. (2005). Shifts in phenology due to global climate change: the need for a yardstick. *Proceddings of the Royal Society B, 272*, 2561-2569

Walther, G.-R., Post, E., Convey, P., Menzel, A., Parmesan, C., Beebee, T.J.C., Fromentin, J.-M., Hoegh-Guldberg, O., & Bairlein, F. (2002). Ecological responses to recent climate change. *Nature, 416*, 389-395

Wang, X., Piao, S., Xu, X., Ciais, P., MacBean, N., Myneni, R.B., & Li, L. (2015). Has the advancing onset of spring vegetation green-up slowed down or changed abruptly over the last three decades? *Global Ecology and Biogeography*, DOI: 10.1111/geb.12289

White, M.A., De Beurs, K.M., Didan, K., Inouye, D.W., Richardson, A.D., Jensen, O.P., O'Keefe, J., Zhang, G., Nemani, R.R., Van Leeuwen, W.J.D., Brown, J.F., De Wit, A., Schaepman, M., Lin, X., Dettinger, M., Bailey, A.S., Kimball, J., Schwartz, M.D., Baldocchi, D.D., Lee, J.T., & Lauenroth, W.K. (2009). Intercomparison, interpretation, and assessment of spring phenology in North America estimated from remote sensing for 1982–2006. *Global Change Biology, 15*, 2335-2359

Woolfson, E. (2013). *Field Notes from a Hidden City*: Granta Publications

Wulder, M.A., & Coops, N.C. (2014). Satellites: Make Earth observations open access. *Nature, 513*, 30-31

Zeng, H., Jia, G., & Epstein, H. (2011). Recent changes in phenology over the northern high latitudes detected from multi-satellite data. *Environ. Res. Lett, 6*

Zhang, X., Friedl, M.A., Schaaf, C.B., Strahler, A.H., Hodges, J.C.F., Gao, F., Reed, B.C., & Huete, A. (2003). Monitoring vegetation phenology using MODIS. *Remote Sensing of Environment, 84*, 471-475

Zhang, X., Tan, B., & Yu, Y. (2014). Interannual variations and trends in global land surface phenology derived from enhanced vegetation index during 1982–2010. *International Journal of Biometeorology, 58*, 547-564

Zhou, L., Tucker, C.J., Kaufmann, R.K., Slayback, D., Shabanov, N.V., & Myneni, R.B. (2001). Variations in northern vegetation activity inferred from satellite data of vegetation index during 1981 to 1999. *Journal of Geophysical Research, 106*, 20069-20083